This is a repository copy of *Transition of a temporally developing three-dimensional turbulent boundary layer*.

White Rose Research Online URL for this paper:
https://eprints.whiterose.ac.uk/205881/

Version: Published Version

Article:
He, S. orcid.org/0000-0003-0326-2447, Lozano-Durán, A. orcid.org/0000-0001-9306-0261, He, J. orcid.org/0000-0002-2340-0694 et al. (1 more author) (2023) Transition of a temporally developing three-dimensional turbulent boundary layer. Physical Review Fluids, 8 (6). 064606. ISSN 2469-9918

https://doi.org/10.1103/physrevfluids.8.064606

Transition of a temporally developing three-dimensional turbulent boundary layer

Shuisheng He [1,*], Adrián Lozano-Durán [2], Jundi He [1], and Minjeong Cho [3]

[1]*Department of Mechanical Engineering, University of Sheffield, Sheffield S1 3JD, United Kingdom*
[2]*Department of Aeronautics and Astronautics, Massachusetts Institute of Technology, Cambridge, Massachusetts 021139, USA*
[3]*Center for Turbulence Research, Stanford University, Stanford, California 94305, USA*

A temporally developing three-dimensional turbulent boundary layer is investigated using direct numerical simulation. The flow is initiated by subjecting a statistically stationary turbulent channel flow to a constant transverse pressure gradient while maintaining the streamwise pressure gradient unchanged. It is shown that this nonequilibrium three-dimensional boundary layer can be described as a turbulent-turbulent transition that is characterized by the development of a laminar boundary layer in an initial turbulent environment followed by a transition to turbulence. Both transient energy growth and crossflow instability may influence the transition, though the former is likely to have a stronger effect when the initial Reynolds number is lower and the transverse pressure gradient is stronger. The transient developments of both the mean flow and turbulence are understood by relating them to the process of transition. The rotation of streaks and the damping effect of the spanwise boundary layer work together to suppress the streamwise and wall-normal turbulence. This effect is stronger than the energy growth in the spanwise direction, causing the overall turbulent kinetic energy and the structure parameter to decrease, explaining the observations made of such flows.

I. INTRODUCTION

Three-dimensional turbulent boundary layers (3DTBLs), in which the mean velocity changes its direction with distance from the wall, are encountered in many engineering applications including, for example, flows around swept wings, wing-body junctions, the bow and stern regions of a ship, and the end walls of turbomachinery or in a curves duct. Such flows may be inviscid induced (traditionally referred to as pressure-driven) flows when the 3DTBL is caused by a spatially varying body force or pressure gradient, such as those found in a curved duct [1], in the upstream of a blunt obstacle [2], or around a wing-body junction [3]. The second category is viscous induced (shear-driven) flow when the three-dimensionality originates from a moving wall. This group includes flows generated due to rotating cylinders [4–9], rotating disks [10,11], and a moving belt or wall [12–14]. This second group also includes channel flows subject to a transverse pressure gradient whose three-dimensionality is similarly caused by viscous diffusion of velocity perturbation near the

---

*s.he@sheffield.ac.uk

wall [15–18]. Earlier work on 3DTBLs has been reviewed by Fernholz and Vagt [19], Eaton [20], and Johnston and Flack [21].

It is also useful to know if a 3DTBL is in equilibrium or nonequilibrium. Some of the above-mentioned flows are in-equilibrium 3DTBLs, including, for example, the flow over a rotating disk studied by Littell and Eaton [10] and Wu and Squires [11], but many of them are in nonequilibrium in the sense that the 3DTBL is either transient or spatially developing in response to an impulsively imposed mean flow perturbation. Hence the terminology nonequilibrium used here has a narrow meaning equivalent to "perturbed" or "nonstationary" as considered by Coleman *et al.* [22]. The physics of this group of 3DTBLs is particularly challenging to explain and predict and is the subject of this paper. In particular, we focus on nonequilibrium viscous induced 3DTBLs.

There are extensive studies of the statistical behaviors, flow similarity, and structural models of the nonequilibrium 3DTBL, but little research has been done on the transitional process from the initial strong nonequilibrium state to the collateral state in which the direction of the mean velocity does not change in the wall-normal direction. The purpose of this paper is to provide insight into the transitional process of the nonequilibrium 3DTBL. We demonstrate that this process is characterized by the development of a laminarlike boundary layer superimposed on the original turbulent flow (which is already well established in the literature), followed by a spontaneous breakup of the boundary layer into higher-Reynolds-number turbulence, that is, a process akin to the bypass transition of a 2D laminar boundary layer subject to a relative high level (greater than 1%) of freestream turbulence. As such, much of the initial nonequilibrium response observed in 3DTBLs can be explained by relating them to the behavior of the strongly perturbed laminar flow before the onset of transition. This hypothesis is inspired by recent work which reinterprets the transient turbulent flow due to a streamwise acceleration from an initial turbulent state as a process of bypass transition to turbulence [23–26]. Below the research on nonequilibrium three-dimensional boundary layer is discussed first, followed by a brief review of some relevant transition literature.

A. Nonequilibrium three-dimensional boundary layer

Nonequilibrium 3DTBLs can be conveniently grouped into spatially developing and temporally developing flows. The former often result from a suddenly applied transverse moving wall. Examples include rotating cylinders studied experimentally by Bissonnette and Mellor [5], Lohmann [6], and Driver and Hebbar [7] and numerically by Jung and Sung [9] and flows over a moving wall or a belt studied experimentally by Kiesow and Plesniak [12,13] and numerically by Kannepalli and Piomelli [27] and Abe [14]. The fundamental structures of the flow due to a rotating wall and a wall moving in a plane are the same, barring potentially some effect of curvature in the first group as noted by Abe [14].

As the fluid encounters the moving wall, a transverse boundary layer is formed, where the mean streamwise vorticity (with the dominant component $\partial W/\partial y$ here) propagates from the wall into the outer region. Kannepalli and Piomelli [27] noted that the streamwise development is characterized by a number of well-defined stages, that is, an initial nonequilibrium two- to three-dimensional boundary layer transition, followed by an approaching-equilibrium (or pseudoequilibrium) flow on the moving wall, and then with the removal of the moving wall, a three- to two-dimensional nonequilibrium boundary layer transition, followed by a process of returning to a 2D boundary layer (2DBL). Lohmann [6] found that after an initial rapid response, the growth of the boundary layer settles to a power-law development with respect to the streamwise distance, i.e., $x^{1/2}$. He compared this behavior with the observation of Antonia and Luxton [28] in a 2DBL following the smooth to rough surface transition and the temporal growth of a laminar Stokes layer, $\delta \propto t^{1/2}$. The suitability of the latter analogy is discussed later in this paper. Along with the growth of the spanwise boundary layer, a deficit in the axial mean velocity is developed near the center of the streamwise boundary layer [6,27]. This was associated with the increasing Reynolds stress and wall shear stress by Lohmann [6] and Kannepalli and Piomelli [27], respectively, whereas more recently Abe [14] associated it with the inviscid skewing. Abe further showed that when the spanwise to

streamwise velocity ratio is 2 or above, the boundary layer thickness θ_z growth rate is larger than $x^{1/2}$, which was associated with the increased eddy viscosity in the spanwise direction.

It is well established that in a nonequilibrium 3DTBL, the streamwise friction coefficient C_{fx} decreases significantly over the initial distance, which is later followed by a recovery and then a plateau that is lower than its 2DBL equilibrium value. The spanwise friction coefficient C_{fz} however increases sharply initially, bounces back somewhat, and then also reaches a plateau more quickly than C_{fx} (see, e.g., [14,27]). At the stage when both friction coefficients have reached a plateau, the flow in the near-wall region remains a constant angle and the structure parameter [$a_1 = \tau/2k$, where $\tau = (\overline{u'v'}^2 + \overline{w'v'}^2)^{1/2}$ and k is turbulence kinetic energy] is close to those of a 2DBL. However, the ratio between the two friction coefficients is still lower than that of the collateral flow and the flow has not reached full equilibrium. This stage corresponds to Kannepalli and Piomelli's pseudocollateral stage. Abe [14] found that it would take significantly longer length for the flow to reach a complete collateral stage (as much as 10 times longer than that initially suggested in [6]). This is mostly due to the slow response of C_{fx}, which was suggested to be intrinsically associated with the inefficiency in extracting energy from the mean flow by the primary Reynolds shear stress $-\overline{u'v'}$ rather than by the secondary Reynolds stress $-\overline{w'v'}$ [14]. A decomposition analysis by Fukagata *et al.* [29] of C_{fx} supported this. The reduced friction also leads to an increase in the momentum thickness in the streamwise flow direction. Abe [14] showed that the friction coefficient reaches the plateau faster (i.e., within a smaller x/θ_0) as the Reynolds number increases. For the same condition, the distance to attain a plateau in [14] is half of that in Lohmann's spinning cylinder. Abe suggested that this is due to the former being more efficient in yielding a 3DTBL.

The turbulent kinetic energy reduces from its 2D value immediately after the leading edge of the moving wall despite the increase in the spanwise stress. Later at the pseudocollateral stage, it recovers and becomes significantly higher than its initial values in the wall region [27]. At the same time, the structure parameter a_1 also decreases greatly near the start of the moving wall, which suggests that the boundary layer is less efficient in extracting shear stresses for the same turbulent kinetic energy. Kannepalli and Piomelli [27] suggested that the reduction in a_1 may be due to the perturbation in the mean flow (i.e., a nonequilibrium effect) rather than the three-dimensional effects *per se*, which agrees well with the transition model discussed herein. In addition, $-\overline{u'v'}$ is smaller than $-\overline{w'v'}$ at the pseudocollateral stage for $U/W = 1$ [14]. The decreased $-\overline{u'v'}$ can also be associated with the lag between the mean strain and the Reynolds stress vectors and thus the anisotropy in the eddy viscosity, which has been observed in a number of studies.

The streaky structures in the viscous wall layer are initially torn by the imposed wall shear causing an immediate reduction in $-\overline{u'v'}$ [14,27]. This effect moves outward at downstream distances. The streaks and vortical structures reappear later and rotate their directions with the surface shear stress. Abe's data [14] appeared to support the structural model of Bradshaw and Pontikos [30], which suggests that the rapid decreases of the shear stress are caused by the sideways tilting of the large eddies away from their preferred orientation. Abe also related the reduced interactions between the inner and outer layers to the inviscid skewing.

By inspecting the spanwise velocity spectra below $y/\delta_{99} = 0.2$, Abe [14] revealed that the most energetic length scale increases linearly with distance from the wall, which indicates a self-similar behavior in the toppling velocity structure. This latter finding supports the self-similar response of a nonequilibrium 3DTBL recently reported by Lozano-Durán *et al.* [18] in a temporally developing 3DTBL. Generally speaking, the law of the wall for the principal flow largely holds with a larger value of the von Kármán constant κ for 3DTBLs.

The second type of nonequilibrium 3DTBL is the temporal developing cases. The flow often starts from a spatially developed stationary channel flow and then a transverse perturbation is applied by a transverse pressure gradient [15,16,18] or a sudden transverse wall velocity on both walls [31] or on one wall [17]. In the case of Coleman *et al.* [22], an idealized 3D velocity distortion was applied to cause the 3DTBL. In all these cases, the flow is homogeneous in both spanwise and streamwise directions and the development occurs over time rather than in space (in the streamwise

direction). Much of the physics observed in the first group of 3DTBL has also been observed in such flows. The delay between the strain and stress and the reduction in turbulence kinetic energy were identified in the pioneering work in [15] and the mechanism was attributed to the reduction in the pressure-strain term in the turbulence budget. Such flows always include an earlier strongly skewed flow development when the streamwise wall shear stress and friction coefficient decrease along with the reduction of turbulence, which is followed by a collateral stage where the stress and strain are approximately aligned with each other near the wall [22,31]. It would however take a long time before the flow finally achieves its equilibrium stage, a new 2DBL (in most of the above studies), or an equilibrium skewed 3DTBL [17]. The latter study noted that the greatest reduction in turbulence drag was obtained when a spanwise shear normal to the main flow was applied in the region $5 < y^+ < 15$ and it was postulated that this result was related to the observation that the maximum turbulence suppression occurs above an oscillating wall at a nondimensional period $T^+ = 100$ [32–34].

For temporal nonequilibrium 3DTBLs, the initial spanwise velocity profile has been found to be well represented by the Stokes solution, but later at the (pseudo)collateral stage it assumes a turbulent profile [15,31]. The reason for the transition was attributed to the reorganization of the turbulence in the skewed direction together with a delayed growth of $-\overline{w'v'}$ by Coleman *et al.* [17], which causes the corresponding development of viscous and semilogarithmic regions in the velocity profile in that direction. The mechanisms for this transition are discussed in detail later in this paper.

Using an idealized three-dimensional distortion to the strain field, Coleman *et al.* [22] established that the adverse pressure gradient rather than the crossflow straining has the strongest effect in causing the reduction of the structure parameter a_1 in the outer flow region, whereas close to the wall the spanwise shear is crucial in causing the nonequilibrium effects. Assuming the wall turbulence is represented by a multiscale collection of wall-attached momentum-carrying eddies, Lozano-Durán *et al.* [18] analyzed the multiscale responses of the structures. The contributions to the turbulent shear stresses of the smallest eddies (closer to the wall) were found to decrease first, followed by those of larger eddies (further away from the wall). With this understanding, the authors demonstrated a self-similar response of the nonequilibrium 3DTBL, which is based on the common characteristic equilibrium velocity and timescale in the early stage of the flow, but at later stages it is replaced by the so-called local-in-time scales.

Various structural models have been proposed to explain the reduction in turbulence and a larger reduction in the Reynolds stress $-\overline{u'v'}$ in both temporally and spatially developing nonequilibrium 3DTBLs. Eaton [35] postulated that the low-speed streaks are inhibited by the mean crossflow, which reduces the ejections and hence the reduction of Reynolds stresses associated with the streak instability and breakdown. On the other hand, several works [10,16,20,31] relate the nonequilibrium turbulence to the strong asymmetry between the vortices of different signs. It has been argued that the imposed transverse mean strain favors either a sweep or an ejection, which ultimately reduces the efficiency of the boundary layer to produce Reynolds stress. Lozano-Durán *et al.* [18] proposed a new structural model for nonequilibrium 3DTBL based on streamwise rolls and streaks at different scales. The imposition of the mean spanwise pressure gradient results in small-scale structures generated under the additional mean shear causing the misalignment between the core of rolls and the flow underneath it, which leads to a less efficient configuration for Reynolds stress production. This model is consistent with that proposed by Lohmann [6], which is also supported by the experimental results of Kiesow and Plesniak [12].

B. Transition

The classical transition scenario of the boundary layer over a flat plate involves the Tollmien-Schlichting (TS) waves, which develop exponentially and become unstable due to nonlinear secondary instability as their amplitudes become higher than a certain threshold, causing the generation of turbulence. This viscous instability develops relatively slowly and is referred to as natural transition. When the freestream turbulence is large (say, greater than 1%), the disturbance

may be amplified rapidly temporarily due to the so-called lift-up mechanism before it is finally dampened by viscosity (i.e., transient growth). The flow with such alleviated disturbances may be susceptible to secondary instability causing the flow to transition into turbulence [36–38]. This scenario of transition is referred to as a bypass transition, as the TS instability is bypassed, and the transition process is often much faster. Due to the frequent occurrences in applications, bypass transition has been studied extensively (see the review articles in [39,40]).

Bypass transition is often described as undergoing three distinct stages, that is, a pretransition stage where disturbances are amplified due to primary instability, a transition stage where secondary instability leads to the generation of isolated turbulent spots which grow and merge with each other, and finally fully turbulent flow after the wall surface is completely covered by turbulence [41]. A notable feature of the pretransition flow is the generation and strengthening of elongated high- and low-speed streaks due to the vertical displacement of fluid particles in a shear flow caused by weak pairs of counterrotating streamwise vortices referred to as the lift-up mechanisms [37,42]. The interactions between the low-speed streaks and high-frequency disturbances are often seen as the source of the secondary instability, leading to the breakdown of the flow to turbulence [43–48]. Andersson *et al.* [42] and Luchini [49] independently analyzed the development of the disturbances in pretransition using optimal disturbance theory and established theoretically that the critical Reynolds number for bypass transition is inversely proportional to the freestream turbulence Tu_0 squared, that is, $Re_c \propto Tu_0^{-2}$. This has been demonstrated experimentally and numerically [50,51] and in addition the length scale of the freestream turbulence has been found to be an important factor in the transition of turbulence [52,53].

In three-dimensional boundary layers, crossflow instability often plays an important role in the transition to turbulence (see the review articles in [54–57]). Differing fundamentally from the viscous TS instability, this instability is inviscid, resulting from the inflectional crossflow velocity profiles, which exhibits a stronger instability than those in a 2DBL. Such instability is dominated by the steady crossflow vortices approximately aligned with the freestream when the initial disturbance is low, but may be strongly influenced by traveling disturbances when the disturbance is high. Once present, the steady crossflow vortices grow until they saturate at an amplitude at an order of 10% of the base flow and the distorted boundary layer is likely to be susceptible to high-frequency secondary instabilities. The secondary instability due to crossflow modes was studied by Malik *et al.* [58] theoretically, White and Saric [59] experimentally, and Bonfigli and Kloker [60] numerically. Such instabilities are of inviscid inflectional type associated with strong shear layers of the mean flow induced by saturated crossflow modes.

It is useful to note that both the lift-up instability contributing to the transient growth in a 2DBL and the crossflow instability are inviscid in nature, and it has been found that under certain conditions the former, algebraic growth, may precondition the flow to provide suitable (and strong) proper initial disturbances to the latter, exponential instability [61,62]. This is not the case in a two-dimensional boundary layer where the output of the transient growth (streaks) bears no resemblance to the TS modes and the former has been found to inhibit the latter [51]. Schrader *et al.* [62] noted that the overshoots of the disturbance energy in a 3DBL transition are often less than those in a 2DBL, which was seen to suggest that crossflow instability destabilizes the flow faster. Under the condition when the transient growth is dominant in their study of spanwise wall oscillations, Hack and Zaki [63] found that the crossflow would redistribute the wall-normal turbulence to the spanwise direction and hence reduce the transient growth rate. Due to the use of a strong noisy environment and the random superposition of different modes in Schrader *et al.* [62], the mean flow deformation was found not to resemble that usually observed under controlled disturbance generation. Crossflow modes of different amplitudes were found to appear side by side in an unpredictable fashion.

Finally, we discuss the transition of a transient turbulent flow. As already mentioned above, He and Seddighi [23,24] demonstrated numerically that the transient process of a flow accelerating from an already turbulent flow caused by the sudden application of an extra pressure gradient is characterized by the development of a laminar boundary layer (superimposed on the existing
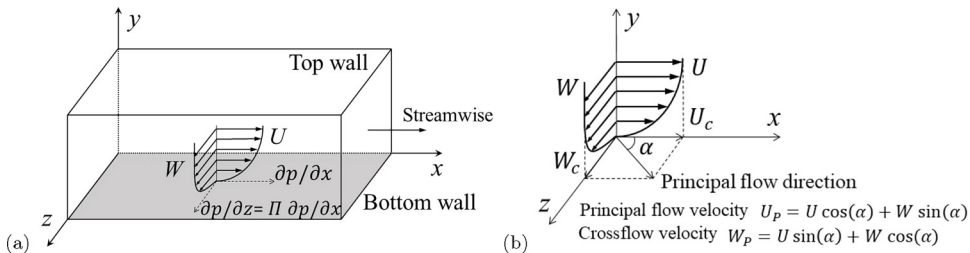
FIG. 1. Schematic diagrams of (a) the computational setup with sketches of the near-wall velocities (not to scale) and (b) the streamwise (U) and spanwise (W) velocities and the principal and crossflow directions in a three-dimensional boundary layer. Here U_c and W_c are centerline velocities. The flow is initially in the streamwise direction only, driven by $\partial P/\partial x$. At the initial time, a constant spanwise pressure $\partial P/\partial z$ is applied while maintaining $\partial P/\partial x$, which causes a three-dimensional boundary layer to form and develop over time. Hence the ratio between the two pressure gradients is a constant Π, i.e., $(\partial P/\partial z)/(\partial P/\partial x) = \Pi$.

turbulent flow), followed by its instability and transition to turbulence. It has been shown that the turbulence does not evolve from the initial state to the new one. Instead, like in a boundary layer transition scenario, the preexisting or newly formed elongated streaks are strengthened with time and eventually become unstable, resulting in isolated turbulent spots generated spontaneously. This new insight into the transient turbulent flow was later confirmed experimentally by Mathur *et al.* [25] and expanded to cover flows over a rough surface [64] and at a higher Reynolds number [65]. Sundstrom and Cervantes [66,67] provided additional experimental evidence and showed that transition also occurs in the acceleration phase of pulsating flows. Jung and Kim [68] investigated the criterion on the acceleration below which the transition phenomenon is insignificant. Most recently, Guerrero *et al.* [26] identified a further inertial phase before pretransition, which is characterized by a rapid and substantial increase in viscous forces together with a frozen behavior of the existing turbulence eddies. They discussed the relatively long and significant period of core relaxation following the completion of transition near the wall. During this period, the near-wall region ($y^+ < 50$) exhibits a quasisteady behavior while turbulence gradually propagates from the wall region to the wake region, which was also identified by He and Seddighi [23].

II. METHODOLOGY

Direct numerical simulations of a temporal nonequilibrium 3DTBL similar to those of Moin *et al.* [15] have been carried out. The three-dimensional transient flow is initialized from a fully developed equilibrium turbulent planar channel flow by suddenly applying a transverse pressure gradient, which is maintained unchanged throughout the transient flow simulation. Additionally, the streamwise pressure gradient is maintained at its initial value. A sketch of the computational domain is shown in Fig. 1.

Three Reynolds numbers are considered, $\mathrm{Re}_\tau = 186$, 546, and 934. Here Re_τ is based on the channel half-height h^*, the friction velocity of the initial flow $u_{\tau 0}^*$, and the kinematic viscosity ν^*. For each Reynolds number, simulations have been carried out for a number of spanwise pressure gradients (see Table I). Results for the two higher-Reynolds-number flows were analyzed in Lozano-Durán *et al.* [18] to study the self-similar response of the flow. Here we analyze those data together with additional lower-Reynolds-number flows to establish insight into the transition process. Detailed numerical methods and case setup can be found in [18], and essential information is outlined below to facilitate discussion.

It is useful to first explain the notation convention used in this paper. Dimensional variables are shown as ( )* and the subscript 0 is used to indicate the value at $t = 0$. Wall units ( )+ are defined in terms of $u_{\tau 0}^*$ and ν^*. Outer units, shown with no subscripts or superscripts, are obtained by normalization using the initial bulk velocity U_{b0}^* and h^* except time, which is scaled by $u_{\tau 0}^*$ and h^*.

TABLE I. Case setup. Here Re_τ is the Reynolds number based on the friction velocity of the initial flow, N_y is the number of wall-normal grid points, N_R is the number of repeated simulations of a case from statistically independent initial flow for an ensemble average, and $\Pi = (dP/dz)/(dP/dx)$. The three series are referred to using their nominal values, that is, 180, 550, and 950, respectively. Cases are labeled as R plus the value of the nominal Reynolds number plus P plus the value of Π, e.g., R180P30, which refers to the case of $Re_\tau = 186$ and $\Pi = 30$. An additional simulation R180P60A with a coarser $N_y = 90$ was carried out (the statistics of which were confirmed to agree closely with those of the corresponding standard case) and the data are used for the purpose of illustration of instantaneous flow behaviors.

Re_τ	y^+	x^+	z^+	N_y	Π	N_R
186	0.15–7.9	9.0	4.5	129	10, 30, 60, 80	10
546	0.26–6.51	8.92	4.46	385	20, 30, 40, 60, 80	10
934	0.35–6.72	7.36	4.29	401	30, 60, 100	5

The streamwise, wall-normal, and spanwise directions are represented by x, y, and z, respectively, and the corresponding velocities are u, v, and w (Fig. 1). Velocities averaged in the homogeneous directions and additionally ensemble averaged over several runs are denoted by U, V, and W, and fluctuating quantities are signified by ( )′. In addition, the principal flow is defined as that in the direction of the centerline of the channel and the crossflow is that normal to it (Fig. 1).

The simulations were carried out using an in-house direct numerical simulation (DNS) code [69]. The incompressible Navier-Stokes equations are discretized using a fully staggered second-order centered finite-difference method in space. The time advancement is performed via a third-order accurate Runge-Kutta method, and the system of equations is solved via an operator splitting approach. Periodic boundary conditions are applied in the streamwise and spanwise directions of the rectangular-channel domain and the no-slip velocity boundary condition is applied at the walls. The code has been validated in previous studies in turbulent channel flows [70] and flat-plate boundary layers [69].

The computational domain is $L_x^* = 4\pi h^*$ and $L_z^* = 2\pi h^*$ for the $Re_\tau = 186$ and 546 cases in the streamwise and spanwise directions, respectively. A larger domain with $L_x^* = 8\pi h^*$ and $L_z^* = 3\pi h^*$ is used for the $Re_\tau = 934$ cases. The suitability of the domain size and mesh resolution (Table I) are discussed in [18].

III. RESULTS

We first show the general flow development for all the cases studied herein in Fig. 2, where the streamwise (U_b) and spanwise (W_b) bulk velocities are shown together with the angles of the total wall shear and the centerline velocity. It can be seen that W_b increases approximately linearly throughout the period of interest in all cases. The reason is that during this early stage of the flow following the imposition of the spanwise pressure gradient, the flow acceleration is approximately equal to the imposed (constant) pressure gradient with the wall friction being much lower than both of them. It is interesting to see that U_b slightly increases initially, but reaches a peak and decreases monotonically afterward, which brings it below the initial value. The initial increase and subsequent reduction of U_b are likely associated with the reduction and increase of the streamwise wall shear stress resulting from the variations of turbulence during these periods, which are discussed in later sections. In contrast, U_b has been found to decrease immediately in moving wall flows, which was explained to be due to inviscid skewing evidenced by the fact that the region of $\partial U/\partial x < 0$ always corresponds to that of $\partial W/\partial x > 0$ [14]. Such spatial variations are absent in the temporal nonequilibrium flow studied herein. Figure 2 also shows that the wall shear angle leads to that of the centerline velocity, with a significant gap between them at the initial stage, but this gap narrows gradually, as expected for such developing three-dimensional boundary layers. The gap between the two angles is very small towards the later stages but in some cases they remain close to a constant
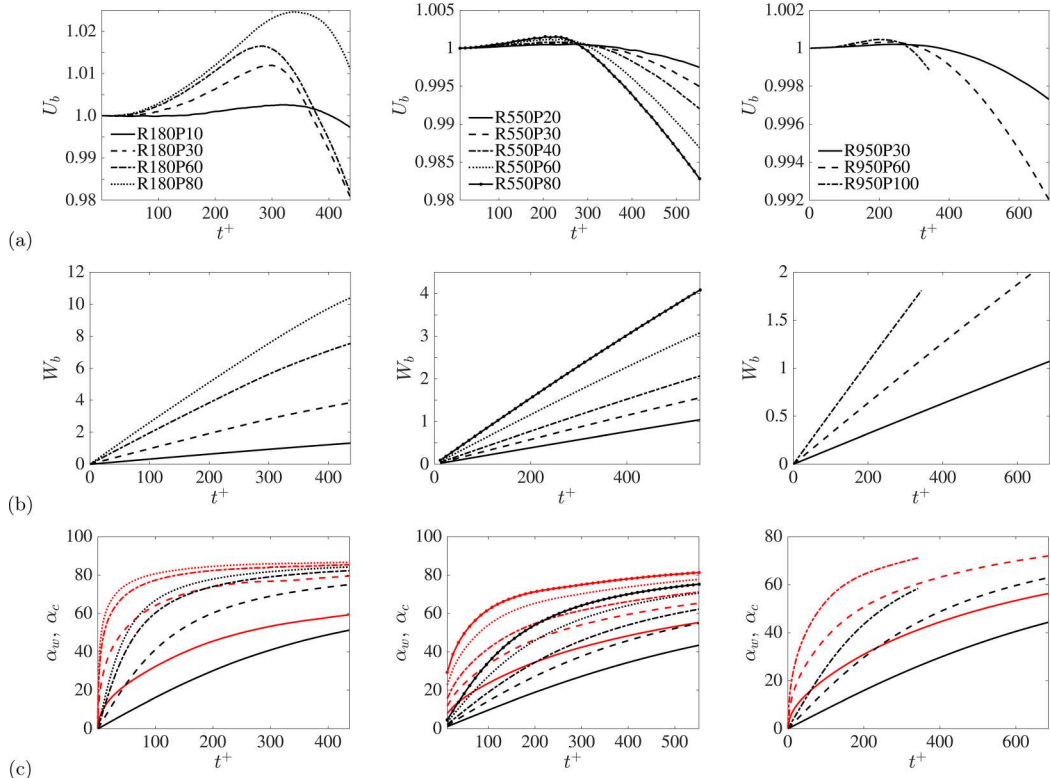
FIG. 2. Overall flow development of all flow cases studied: (a) the streamwise bulk velocity, (b) the spanwise bulk velocity, and (c) the angle in degrees of the wall shear α_w (red lines) and that of the centerline velocity α_c to the streamwise flow (black lines).

within the time studied. The flow is described as being strongly in nonequilibrium when the angle difference is significant, but towards the final stage, when the angle gap is diminished, the flow is said to have reached a state of the approximate or pseudocollateral stage [14,15,71].

A. Observation of transition

The response of the instantaneous flow following the imposition of a constant transverse pressure gradient is visualized in Figs. 3–5. Figure 3 shows contours of the instantaneous spanwise fluctuating velocity in a wall parallel plane at $y^+ = 3.76$ for a number of times in case R180P60A. The first observation is the formation of new tilted streaks up to t^+ $(=t^* u_\tau^{*2}/\nu^*) = 270$ and that their angles increase with time. The latter is clearly due to the rotation of the total mean flow with time under the influence of the transverse pressure gradient. The second observation is the formation of isolated turbulent spots, first appearing at around $t^+ = 260$. At $t^+ = 270$, multiple spots are clearly observed. Later these spots grow and connect to each other, covering larger areas. The entire domain is populated by new turbulence at $t^+ = 350$. Turbulent spots can be visualized in many cases studied herein, but it becomes more difficult in flows of a higher initial Reynolds number and a lower transverse pressure gradient, as expected.

The process of formation of elongated streaks followed by the generation of isolated turbulent spots described above resembles that in the laminar-turbulent bypass transition of a boundary layer over a flat plate subjected to a relatively high freestream turbulence [41,72,73]. Based on this observation and the results presented later in this paper, we demonstrate that the nonequilibrium
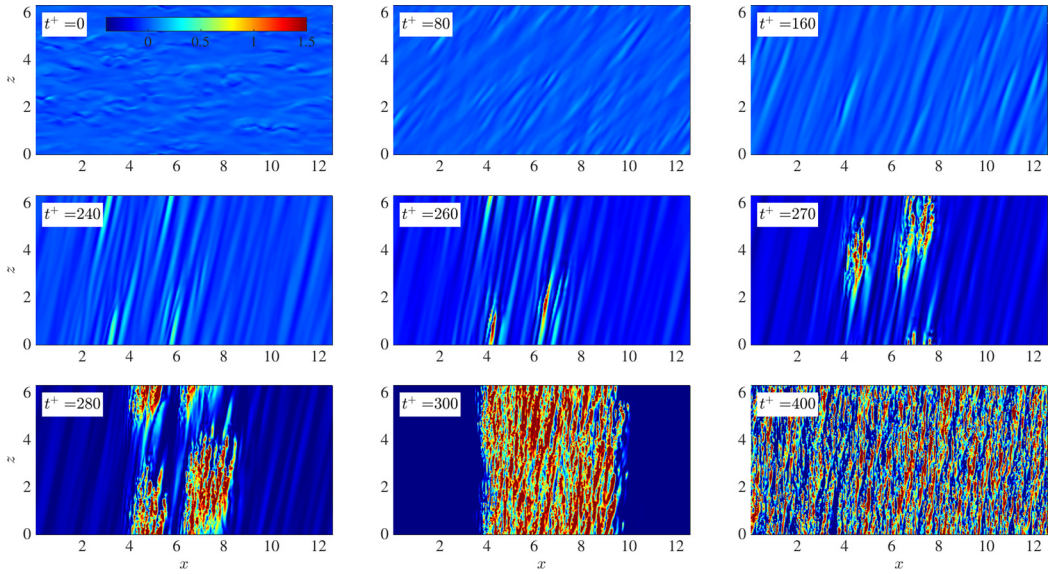
FIG. 3. Spanwise fluctuating velocity w' in an xz plane with $y^+ = 3.71$ in case R180P60A. The range of the color bar was selected to highlight the new streaks created during the transition.

three-dimensional boundary layer considered herein is characterized by a buffeted laminar boundary layer developed in the spanwise direction followed by its transition to turbulence, even though the initial flow is already turbulent. This transitional framework for nonequilibrium 3DTBLs expands the theory initially established by He and Seddighi [23,24] for axially accelerating turbulent flow to a more complex three-dimensional flow scenario.

Additional evidence for transition is shown in Fig. 4, which displays the time development of the instantaneous velocities u and w along a horizontal line across the span of the channel. The streamwise fluctuating velocity remains largely unchanged whereas the spanwise fluctuating velocity increases slowly but steadily. This continues until about $t^+ \approx 200$, when there are abrupt increases in both velocity components but which die away shortly after. This response is likely due to turbulent spots crossing the probing line. Later at $t^+ = 240$, strong fluctuations occur again in both u and w which are sustained thereafter. At this stage, the sudden changes in the amplitudes are also accompanied by discontinuous changes in the time and spatial scales (in the horizontal and vertical abscissas, respectively). Both scales undergo a sudden reduction, suggesting that the flow switches from an initial lower-Reynolds-number state to one of a higher-Reynolds-number state. This observation reinforces the transitional nature of the three-dimensional boundary layer.
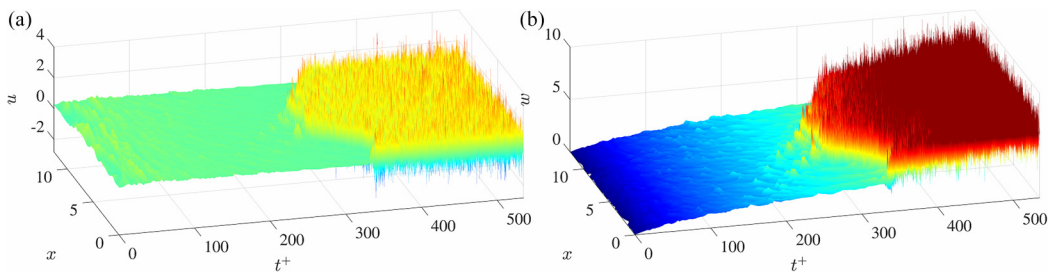

FIG. 4. Variation of the (a) streamwise and (b) spanwise velocities along a horizontal line along the channel at $y^+ = 8$ (case R180P60A).
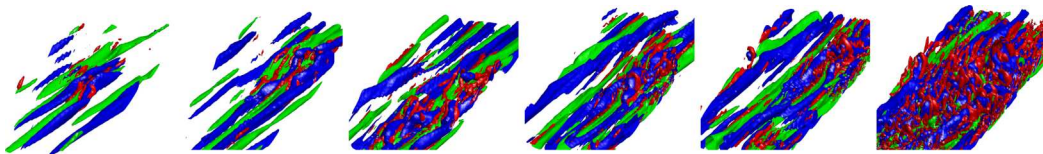
FIG. 5. Formation of a single turbulent spot illustrated with isosurfaces: blue (dark gray), $u' = -0.3$; green (light gray), $u' = 0.3$; and red (deep dark gray), $\lambda_2 = -5$ (case R180P60A). The time instants from left to right are $t^+ = 220, 242, 255, 262, 266, 279$.

Figure 5 shows the development of a single turbulent spot over time using isosurfaces of streamwise fluctuating velocity and λ_2, where λ_2 is the second largest eigenvalue of the symmetric tensor $\mathbf{S}^2 + \mathbf{\Omega}^2$ ($\mathbf{S}$ and $\mathbf{\Omega}$ are the symmetric and antisymmetric parts of the velocity gradient tensor ∇u). After the observation of a turbulent spot, we trace back both in time and upstream location to identify the source of the initial instability. In this case, the turbulence spots appear to result from the instability around a low-speed streak similar to those often observed in the bypass transition (see, e.g., [43,44,46]).

Despite nonequilibrium 3DTBLs not typically being described in terms of transition, many phenomena observed in previous studies can be seen to support this proposition, including the breakup of the streamwise streaks into small pieces, the reformation or alignment of the streaks along the new wall shear direction, and finally the coalescence to take an elongated shape as described in both temporal nonequilibrium 3DTBLs [17] and spatially developing 3DTBLs [14,27]. The latter two papers also clearly showed the disappearance and formation of new vortical structures during the transitional period using low-pressure isosurfaces superimposed on the wall enstrophy [27] or Q criterion [14]. The sequence of events found in both studies is very similar to that described herein. Following the imposition of the spanwise motion, the near-wall streaky structures and the quasistreamwise vortices were initially found to be weakened. Kannepalli and Piomelli [27] noted that this effect is initiated first near the wall but propagates away from it. Further downstream, new vortical structures are generated at the wall and again convected towards the outer layer. The quasistreamwise vortices are now oriented in the direction of the wall shear stress, at an angle of approximately $50°$ to the streamwise direction [27]. Abe [14] attributed the above process to the nonequilibrium effect and found that the reduction of the vortical structures and regeneration of the new structures are more pronounced with increasing speed of the wall. He also noted the clustering of near-wall vortices especially with larger wall movements, which suggests the formation of turbulence spots associated the early stage of transition.

B. Time developing transverse boundary layer

Following the application of the transverse pressure gradient, the flow in the entire channel accelerates uniformly in this direction as a plug flow except in the vicinity of the wall where the no-slip boundary condition applies due to viscosity. In this region, the velocity of the fluid decreases rapidly from the bulk value to zero at the wall. Consequently, a thin boundary layer is formed, which grows away from the wall with time. The initial laminar behavior of this boundary layer has been well established. In temporal nonequilibrium 3DTBLs, the mean spanwise velocity profile collapses close to the Stokes solutions [15,17,31] in the first phase, but deviates from it later. It has also been noted that for a spatially developing flow, the boundary layer development can also be related to $x^{1/2}$ at a certain stage, implying that the flow is similar to the Stokes layer [14]. This latter point is not exactly accurate, as discussed later in this section.

To study the behavior of boundary layer in the present flow, we compare it with the corresponding laminar flow caused by the same flow acceleration. This is an extended Stokes first problem where the mass flow rate increases with time in a nonuniform way, rather than a step change as in the classical Stokes problem. The solution of this problem provides the time developing velocity
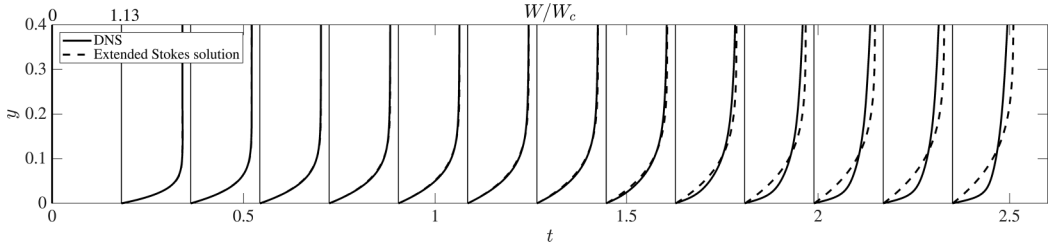
FIG. 6. Spanwise velocity profile development in R180P60 and comparison with the solution of the extended Stokes first problem for an equivalent laminar acceleration. Here W_c is the centerline velocity.

as [74]

$$W(y, t) = \int_0^t W_b'(\tau) \text{erfc}\left(\frac{y}{2\sqrt{\nu(t - \tau)}}\right) d\tau,$$ (1)

where erfc is the complementary error function and $W_b'(t)$ the bulk flow acceleration.

Figure 6 shows the comparison between the spanwise boundary layer obtained from the DNS and the Stokes laminar solution for case R180P60 as an example. The two profiles agree closely during the pretransitional phase until around $t = 1.2$ (i.e., $t^+ = 223$), after which they deviate from each other. At this stage, the DNS result assumes a fuller profile, which is representative of a turbulent flow. The time when the deviation occurs corresponds roughly to the onset of transition observed in Figs. 3–5. During the initial pretransitional period, the streamwise velocity remains largely unchanged (not shown).

The overall behaviors of the transverse boundary layer can be depicted using the integral parameters, such as the friction coefficient C_f, the displacement or momentum thickness δ or θ, respectively, and the shape factor H. The integrations for the calculation of δ and θ are nominally to the channel center, though the transverse flow is uniform in most of the channel in the early stages that are of most interest (see Fig. 6). The results are shown in Figs. 7–9. These plots are especially useful as their behaviors in laminar and turbulent flows are distinctly different and well known. The onset of transition is marked in each case using the minimum streamwise friction coefficient C_{fx}, which corresponds to the time when turbulence spots are observed to appear (see, e.g., Figs. 3–5). It is noted that in the 3DTBL concerned here, the streamwise friction factor C_{fx} is more appropriate for this purpose than the spanwise friction coefficient C_{fz} since the variation of the former is mostly influenced by turbulence whereas the latter (or, similarly, the total friction coefficient C_f) is also influenced by the growth of the new boundary layer. Other effective indicators for the onset of transition are the time when the streamwise or wall-normal turbulence stresses reach their minimum values, since they decrease in the pretransition stage and only start increasing again after the onset of transition, as discussed later. There are some differences between the values of onset of transition depending on how promptly particular quantities respond to the generation of new turbulence, but the difference between them is generally insignificant. The minimum C_{fx} is used throughout this paper.

Figure 7 shows the development of the friction coefficient in the streamwise and spanwise directions, defined as $C_{fx} = \tau_{w,x}^*/0.5\rho^* U_b^{*2}$ and $C_{fz} = \tau_{w,z}^*/0.5\rho^* W_b^{*2}$, respectively. The figure shows that C_{fx} decreases during pretransition, which can be related to the initial (partial) laminarization, to be shown later and also reported in previous studies (e.g., [15]). The stronger the acceleration, the stronger the reduction in C_{fx}, and the trend is reversed following the transition. Similar trends of reduction and recovery of C_{fx} were also observed in spatially nonequilibrium 3DTBLs [14,27].

Assuming the flow is laminarlike, the friction coefficient for the spanwise boundary layer can be obtained from the solution of the extended Stokes problem as

$$C_f = \frac{2}{W_b^2} \int_0^t W_b'(\tau) \sqrt{\frac{\nu}{\pi(t - \tau)}} d\tau.$$ (2)
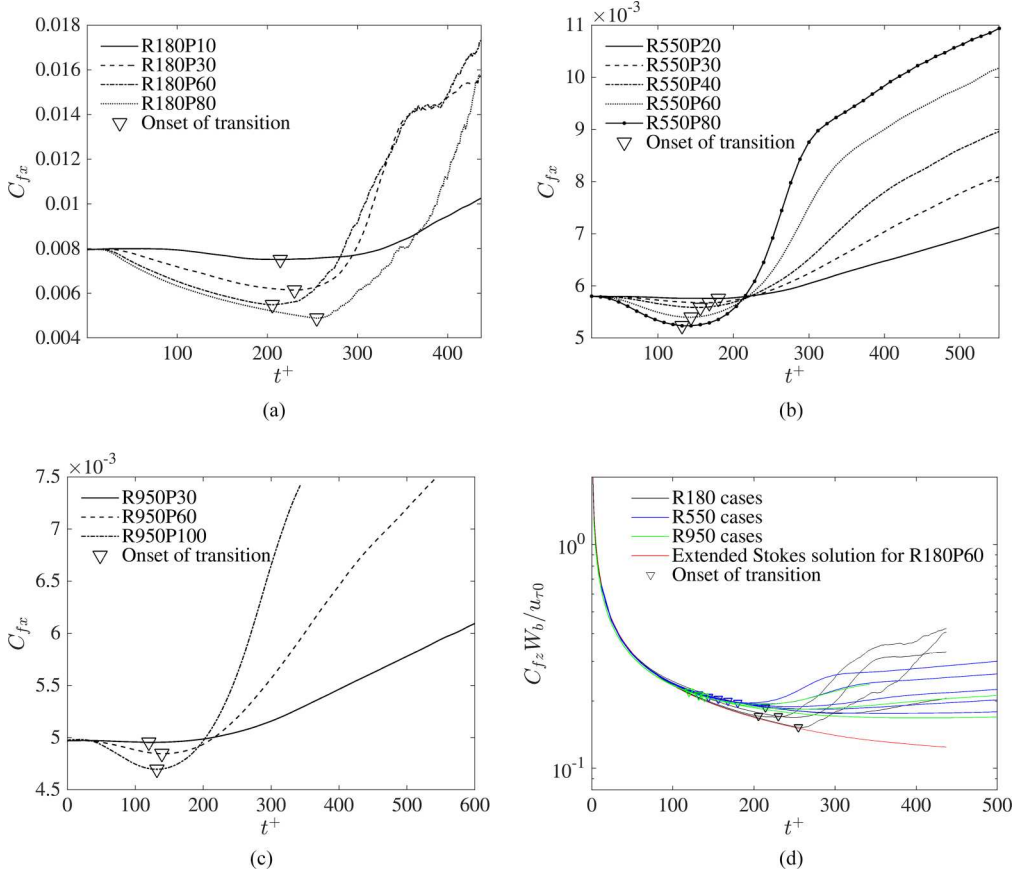
FIG. 7. Friction coefficient in the (a)–(c) streamwise and (d) spanwise directions. The triangle markers show the onset of the transition detected using minimum C_{fx}. Also shown in (d) is the extended Stokes flow solution for R180P60 as an example and solutions for other cases are only slightly different due to the small differences in their acceleration rates.
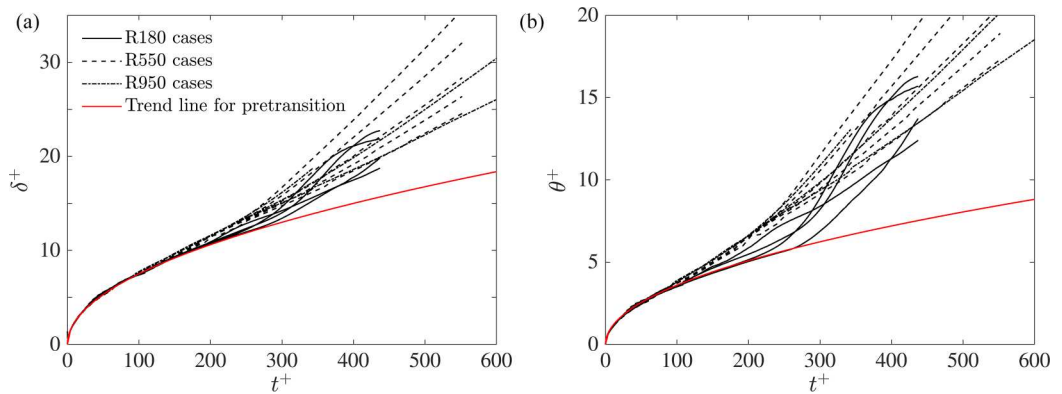

FIG. 8. (a) Displacement and (b) momentum spanwise boundary layer thickness. The red lines are trend lines for the pretransition stage in the form of $\delta^+, \theta^+ \propto (t^+)^{1/2}$. The proportion factors are (a) 0.75 and (b) 0.36, chosen to fit the data.
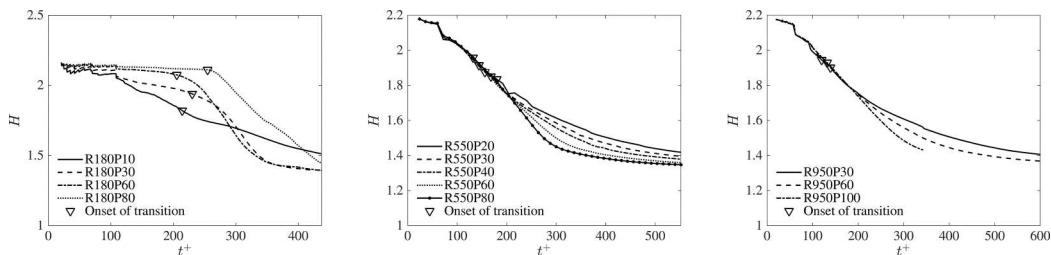
FIG. 9. Boundary layer shape factor. The onset of transition detected using minimum C_{fx} is shown triangle markers.

If we additionally take into account the fact that the initial acceleration (pretransition) of the flow is approximately constant, then the friction coefficient can be approximated by $C_f \approx \frac{2}{W_b^2} W_b' \sqrt{\nu t/\pi}$ or $C_f \approx (2\sqrt{\pi})(u_{\tau 0}/W_b)/\sqrt{tu_{\tau 0}^2/\nu}$ considering $W_b = W_b' t$. This expression implies that the initial response of the renormalized friction coefficient $C_{fz}(W_b/u_{\tau 0})$ as a function of t^+ for all cases should be brought together to align with the Stokes solution if the initial flow is laminarlike. It can be seen from Fig. 7(d) that this is indeed the case supporting the assumptions made above. It is useful to note that the laminarlike response of the C_f in a streamwise accelerated turbulent flow was discussed in some detail by He and Ariyaratne [75] and He *et al.* [76] based on computational and experimental data, respectively, and later by He and Seddighi [23,24] with respect to transition.

The developments of the displacement and momentum boundary thickness of the spanwise flow are shown against t^+ in Fig. 8, which shows that the data from all cases are reasonably close. They are in good agreement with the development of the Stokes first problem, that is, $\delta, \theta \propto (\nu t)^{1/2}$, or equivalently $\delta^+, \theta^+ \propto (t^+)^{1/2}$, in most of the pretransition stage. Towards the later part of this stage, the boundary layer (especially the momentum boundary θ) appears to deviate from the Stokes solution, which is likely due to the effect of the preexisting turbulence. Following the onset of transition, the boundary layer thickness increases rapidly, showing a typical transition behavior. The rate of increase at this stage is dependent on the spanwise pressure. The stronger the pressure, the higher the Reynolds number at transition and in turn the stronger the new turbulence, which leads to a faster increase in the boundary layer thickness.

The development of the shape factor of the boundary layer (H) also shows a typical behavior of bypass transition. The value of H is initially around 2.1 in all cases, which is lower than the typical value of about 2.5 for a canonical boundary layer, likely due to the fact that the freestream velocity of the flows concerned here starts from zero and increases linearly with time [see Fig. 2(b)]. At the onset of transition marked using minimum C_{fx}, the value of H is around 1.9 in most cases, which is reasonably consistent with that in the 2DBL bypass transition in terms of relative reduction of H being around 15% [41,72]. Exceptions to this are R180P80 and 60, where the pretransition lasts longer and the transition occurs much more rapidly. Here the shape factor only starts decreasing at the time of onset of the transition.

For spatially developing 3DTBLs, Kannepalli and Piomelli [27] and Abe [14] noted that the spanwise boundary layer first develops rapidly, but after a short distance, the growth rate of the momentum boundary layer thickness settles to a power law proportional to $x^{1/2}$. The latter was related to the molecular diffusive process, similar to the $\theta \propto t^{1/2}$ behavior observed for the laminar Stokes layer. Even though this appeared to be consistent with the temporal development discussed above, it is actually misleading. The region where this $x^{1/2}$ law was identified is in fact towards the later part of the moving wall where the transition to turbulence is expected to have already occurred. The first region, where the boundary layer was described as responding fast, is in fact close to the $x^{1/2}$ development and hence corresponds to the laminar Stokes solution. Towards the end of this region, the boundary layer growth becomes faster, which can be interpreted as being influenced by
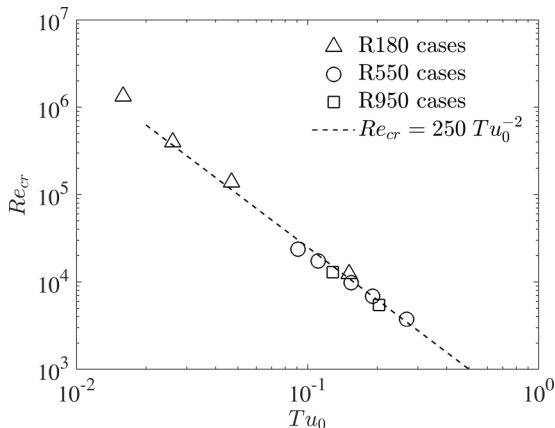
FIG. 10. Critical Reynolds number versus freestream turbulence intensity. The dashed line is a best-fit curve of the data.

the transition to turbulence. Taking the cases $Re_\theta = 300$ and 600 with $W_S/U_0 = 1$ (where W_S is the spanwise moving wall velocity and U_0 the incoming streamwise flow velocity) of Abe [14] as examples, the transition between the two regions occurs at around $x/\theta_0 = 150$ and 140, respectively. These are at the locations where the friction factor has passed its minimum and started recovery in each respective case. Consequently, the boundary layer development in the spatially developing 3DTBLs also appears to show an initial laminarlike response followed by a transition to turbulence.

C. Transition mechanisms

As discussed earlier, it has been established experimentally, computationally, and through transient growth theory that the transitional Reynolds number for the two-dimensional boundary layer bypass transition is related to the freestream turbulence Tu_0 via a power law $Re_{cr} = C(Tu_0)^{-2}$, where C is a constant. A few things need to be considered in order to assess the suitability of this relationship for the present flow. First, the freestream velocity of the transient flow following the imposition of the transverse pressure is not constant but increases with time; consequently there is some flexibility in defining the reference velocity. Here we use the centerline velocity at the time of transition, noting that a further increase in velocity is irrelevant to the onset of transition. Second, the streamwise distance needs to be defined in such a temporal acceleration flow and here we use the convection distance between the start of the application of the transverse pressure and the onset of transition, that is, $x_{cr}^* = \int_0^{t_{cr}^*} W_b^* dt^*$, where t_{cr}^* is the time at the onset of transition determined using minimum C_{fx}. Finally, there is also a flexibility in the definition of freestream turbulence as the preexisting wall shear turbulence is nonuniform spatially and is anisotropic in nature. Here we use the maximum value of the turbulence intensity to characterize turbulence of the initial flow.

Based on the above discussion, the (equivalent) transitional Reynolds number Re_{cr} and the freestream turbulence intensity Tu_0 can now be written as

$$\text{Re}_{cr} = \frac{x_{cr}^* W_{b,cr}^*}{\nu^*}, \quad Tu_0 = \frac{\max_y[(2/3k_0)^{1/2}]}{W_{b,cr}^*}, \tag{3}$$

where k_0 is turbulence kinetic energy at $t = 0$ and $W_{b,cr}^*$ is the spanwise bulk velocity at t_{cr}^*. Figure 10 shows Re_{cr} versus Tu_0 for all cases studied here. It can be seen that the data are very well represented by $Re_{cr} = C(Tu_0)^{-2}$ with $C = 250$, which is reasonably close to that of Fransson's value $C = 196$ for the bypass transition over a flat plate [77]. We note, however, a direct comparison of the exact values of C is not particularly relevant considering the flows being very different and
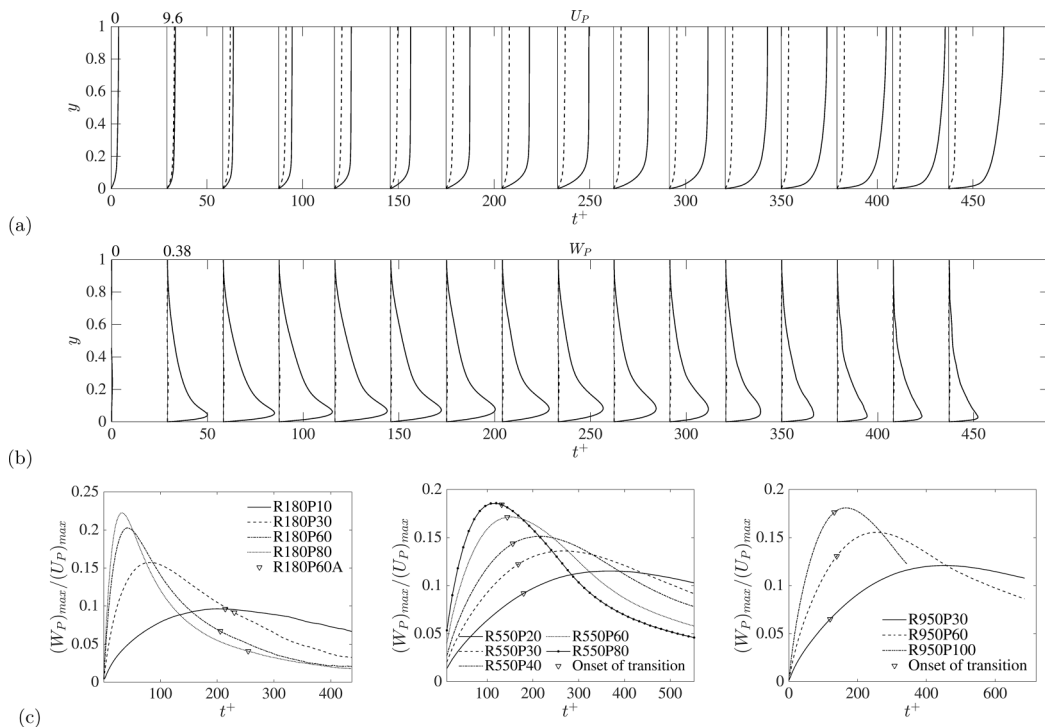
FIG. 11. Development of the velocity profiles (a) along the centerline velocity direction U_P (principal flow) and (b) perpendicular to it W_P (crossflow) in case R180P60. Dashed lines show the initial flow and solid lines profiles at t. (c) Relative crossflow strength $(W_P)_{\mathrm{max}}/(U_P)_{\mathrm{max}}$ in all cases.

the uncertainties in the definition of the relevant parameters in 3DTBLs due to the transient flow behavior discussed above.

There are two potential transition mechanisms which may occur in a three-dimensional boundary layer with relatively high disturbances such as that considered herein, that is, (i) bypass transition due to transient growth of the disturbances existing in the initial flow [41,72] and (ii) crossflow instability due to an inflectional velocity profile resulting from the application of the transverse pressure gradient [56,57,62]. After the application of the transverse pressure gradient, the mean flow starts rotating in the spanwise direction, that is, the mean velocity at any location continues changing its direction with time (from streamwise to spanwise directions). The flow however rotates at different rates at different wall distances due to the effect of viscosity, which leads to the so-called crossflow. We use the direction of the velocity in the channel center to represent the principal flow U_P and the flow perpendicular it to represent the crossflow W_P. As shown in Fig. 11(a) for case R180P60, the principal flow initially increases relatively slowly, but it speeds up in the second half of the pretransition period, reaching a level that is more than double its initial value at around $t^+ = 100$. In contrast, the crossflow [Fig. 11(b)] appears to be established quite quickly, reaching its peak soon after $t^+ = 50$, after which the crossflow (both the amplitude and the extent) appears to be largely unchanged until the transition, while the W_P continues increasing at approximately a constant rate during all this time. Consequently, relative to the principal flow, the crossflow strength decreases with time following an initial increase. This general trend of crossflow development is seen in all flow cases, though the details can be significantly different in different cases.

We introduce a measure of the strength of the crossflow using the ratio of the maximum W_P over the maximum U_P velocities, which is shown in Fig. 11(c) for all the cases studied. It can be seen that the relative strength of crossflow in all cases increases initially, reaching a maximum at
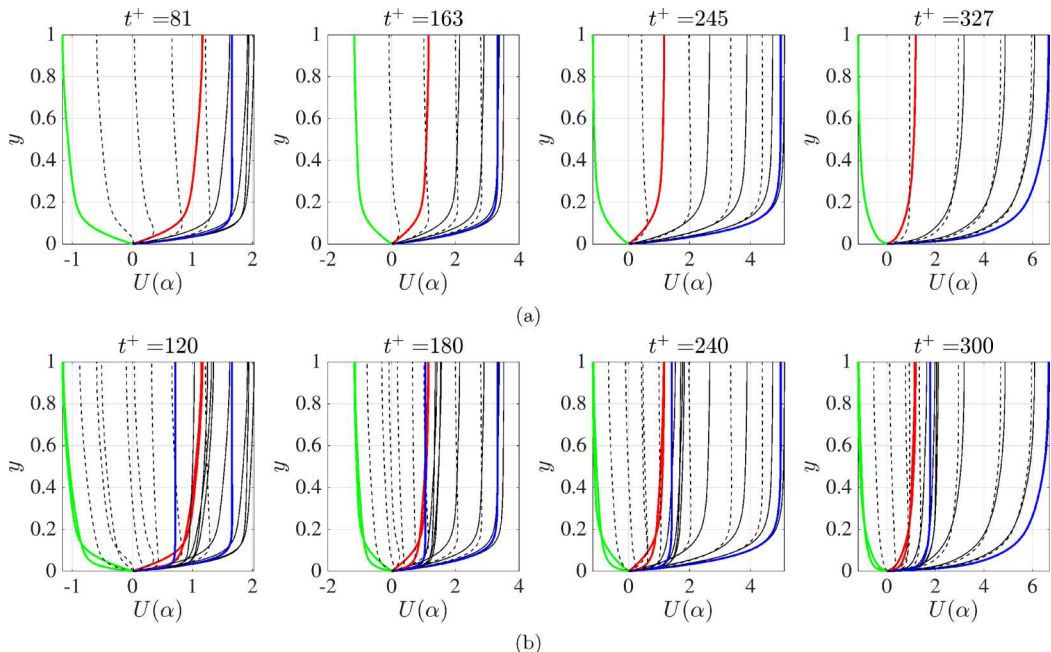
FIG. 12. Directional velocity profiles at several time instants in cases R180P60 and R550P60. These directional velocities are on a plane at an angle α to the x axis, where $\alpha = 0$ (red lines), $\alpha = 0.5\pi$ (blue lines), $\alpha = \pi$ (green lines), $\alpha = 0.1\pi, 0.2\pi, 0.3\pi, 0.4\pi$ (black solid lines), and $\alpha = 0.6\pi, 0.7\pi, 0.8\pi, 0.9\pi$ (black dashed lines).

some stage, and decreases afterward. The higher the transverse pressure gradient, the stronger the crossflow relative to the principal flow and the earlier it reaches the maximum strength. For most cases studied here, the transition occurs at a location where the crossflow is strong and close to its maximum value. Exceptions to this are cases R180P60 and P80, in which the crossflow has long passed its peak value and decreased to a much lower level. Hereafter, we put these latter two cases together as group A and the rest of the cases as group B. The above result, together with those presented later, appears to suggest that the transition of group A cases is likely to be more strongly influenced by transient growth, whereas group B cases are potentially strongly influenced by exponential growth (crossflow), though R180P30 is somewhere in between the two groups.

Crossflow instability can be investigated by studying the directional velocity profiles, defined on vertical planes at different angles to the main flow direction [56] and the most unstable of such profiles with the strongest inflection points are likely to be the active cause for transition. In the present case, the directional velocities vary with time. Such velocities are shown in Fig. 12 for a number of times for cases R180P60 and R550P60. Some directional velocity profiles in the pretransition phase clearly show an inflectional point within the boundary layer region in both cases. In case R180P60, strong inflections are only observed at early times and the directional velocities show very weak inflections later over a period before the transition, say, $t^+ = 200$–300 (not all data are shown in the figure). In contrast, in case R550P60, profiles with a strong inflection point are observed during the entire pretransition period. This observation is consistent with the crossflow strength shown earlier in Fig. 11. Together these data suggest that the flows in group B may be strongly influenced by crossflow instability, whereas those in group A may not be.

One of the crossflow instability characteristics is the formation of corotating vortices. Such vortices have been observed at some stages of the pretransition phase in all cases examined. Figure 13 shows the instantaneous flow on the zy plane and $t^+ = 100$ in case R180P60A.
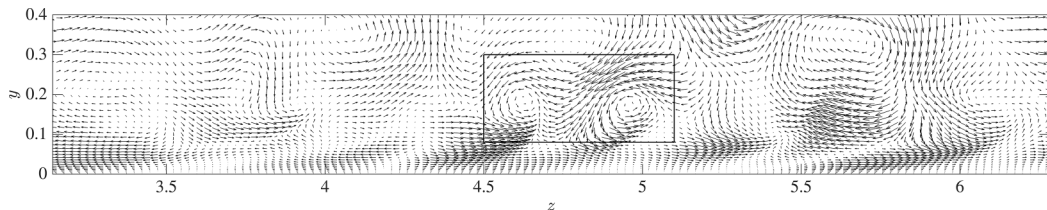
FIG. 13. Fluctuating velocity vectors w' and v' in a zy plane at $t^+ = 100$ in case R180P60A with corotating vortices identified.

Multiple corotating vortices can be clearly identified, despite the strong background noise due to the high level of disturbances. Such corotating vortices however disappear well before the onset of transition and therefore this again suggests that for such cases (group A), the crossflow instability is present at some stages of the 3DTBL but it likely plays an insignificant role, consistent with Fig. 11.

D. Turbulence statistics and energy growth

Here we study the transient developments of turbulence in the 3DTBLs in relation to the process of transition. Figures 14 and 15 show the wall-normal profiles of the turbulence stresses and the structure parameter a_1 at a series of time points in case R180P60 as an example. In this flow, the transition begins at around $t^+ = 200$ and is completed at around $t^* = 350$ based on the minimum C_{fx} and the first peak that follows, respectively (see Fig. 7). It can be seen that the streamwise turbulence stress $\overline{u'^2}$ decreases significantly during the pretransition period but starts to increase rapidly following the onset of transition, reaching a level close to its maximum when the transition is completed. The pretransition reduction of $\overline{u'^2}$ can be partially linked to the destruction of the preexisting streaks aligned in this direction, as shown in Fig. 3 and also in previous studies [14,15,27]. The crossflow tends to enhance the vortices with a sense of rotation conforming with it but weakens those with a rotation sense against it. The resultant effect is that vortical pairs are weakened as a whole, which are known to be linked to streaks weakening and destruction [78]. The second reason is the shear-sheltering effect due to the new transverse boundary layer, which tends to attenuate high-frequency vortical perturbations [79,80]. Such an effect plays an important role in the boundary layer bypass transition [40,41], in which the boundary layer tends to dampen the small-scale disturbances but allows the larger-scale disturbances to penetrate through, facilitating the generation of new streaks through transient growth. The flow is more complex in the present flow, where the perturbations, that is, turbulence, already exist in the flow whereas the new boundary layer is moving outward, entraining the perturbations due to the relative movements. In this regard, it is of interest to note the work by Hunt and Durbin [79], who studied various general flow conditions, including a mean shear flow introduced (at $t > 0$) into a preexisting field of inhomogeneous turbulence. They demonstrated that the fluctuations in all three components decrease exponentially below the interface. This model problem is significantly simpler than the 3D flow problem concerned here, but it nevertheless provides a plausible explanation to our observations, though further study is needed to gain a better understanding of the process.

The wall-normal component $\overline{v'^2}$ behaves in a similar way to $\overline{u'^2}$, decreasing during pretransition but at a much lower rate. This reduction can largely be related to the shear-sheltering effect due to the spanwise boundary layer, whereas the effect on this wall-normal component from the evolution of the streaks turning spanwise from its initial streamwise alignment is relatively small. In contrast, the spanwise turbulence $\overline{w'^2}$ increases steadily with time during pretransition, which can be linked to the formation and strengthening of the new streaks that tend to be increasingly more
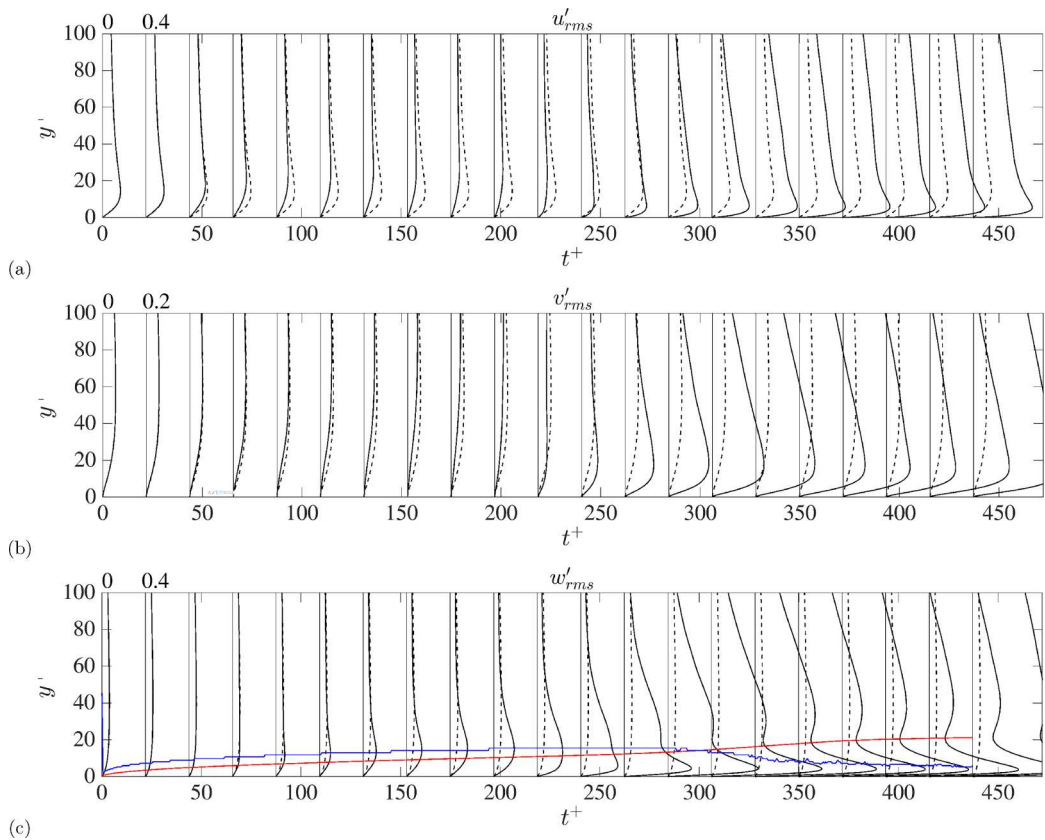
FIG. 14. Root mean square of the fluctuating velocities (a) u'_{rms}, (b) v'_{rms}, and (c) w'_{rms} in case R180P60. The black solid lines are profiles at various t^+ and the dashed lines are the initial profiles at $t^+ = 0$ for comparison. The blue and red lines show the locations of the peak crossflow and the displacement boundary layer thickness, respectively.

aligned with the spanwise direction. The peak of the wall-normal profile at any time is located just outside the boundary layer displacement thickness, which is typically seen in the bypass transition resulting from transient growth as observed experimentally and computationally [50,72] as well as demonstrated theoretically through analyzing optimal perturbations [42,49]. It is also interesting to note that these peaks appear to be just below the locations of the peak crossflow as shown in Fig. 14(c). A further interesting point to note is that two local peaks have developed in $\overline{w'^2}$ following the onset of transition. The peak closer to the wall is clearly associated with the newly generated turbulence at a higher Reynolds number. This location is significantly lower than that during the pretransition which is linked to the streaks, showing the different natures of the w' before and after transition. It is however interesting that the outer-region peak is also growing stronger during and even after the completion of the transition as it moves away from the wall. This is possibly linked to the continuing increase of the spanwise flow W_b (Fig. 2). Double peaks are also seen in R180P80 but not in group B flows.

During pretransition, the primary turbulent shear stress $-\overline{u'v'}$ decreases progressively due to the reduction of u' and v' discussed above, reaching a very low level at the end of this period showing strong laminarization (Fig. 15). In contrast, $-\overline{w'v'}$, which is zero in the initial 2D flow, gains a small value during this time. Following the onset of transition, both stresses increase rapidly, first near the wall, but progressively spreading further away. The $-\overline{w'v'}$ reaches a much higher level than $-\overline{u'v'}$ at
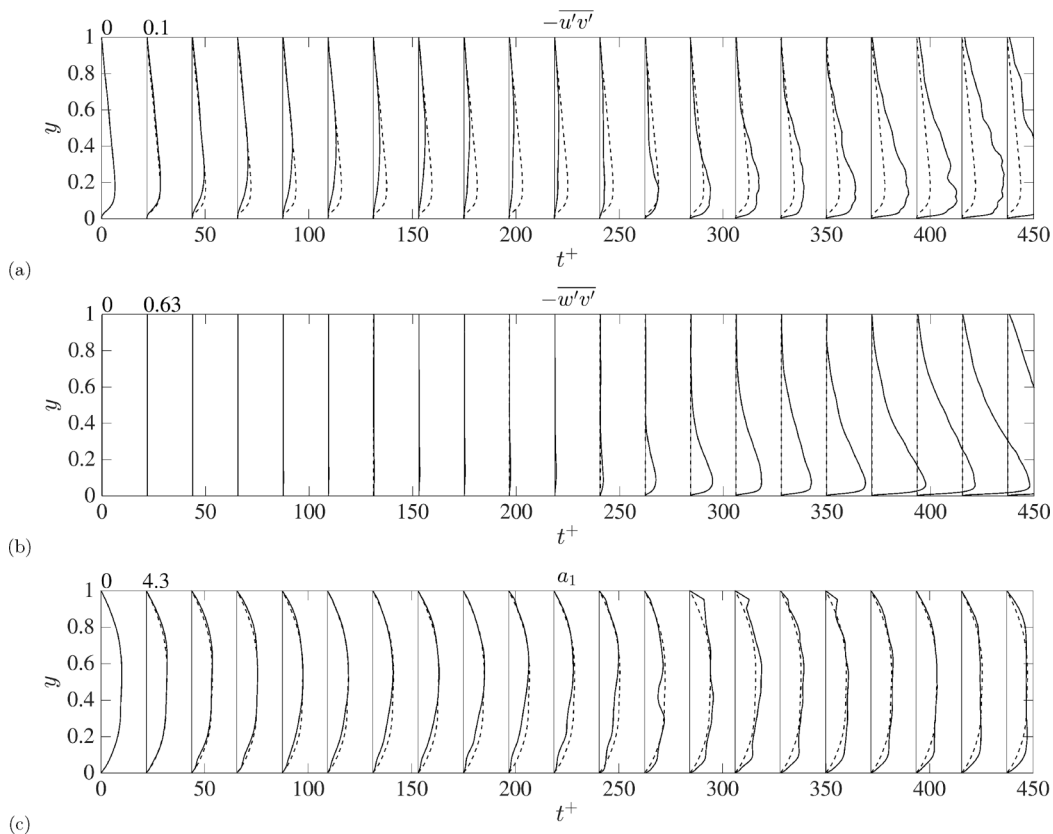
FIG. 15. Turbulent shear stresses (a) $-\overline{u'v'}$ and (b) $-\overline{w'v'}$ and (c) structure parameter a_1 in case R180P60. The black solid lines are profiles at various t^+ and the dashed lines are the initial profiles at $t^+ = 0$ for comparison.

the end of transition. It should be noted that even when the transition has completed, the distributions of both $-\overline{u'v'}$ and $-\overline{w'v'}$ are still far from that of a typical shear stress with the development in the core still to happen. A relaxation period follows during which the newly generated turbulence propagates into the core [23,26].

It is known that the structure parameter a_1 $(\equiv \tau/q)$, where $\tau=(\overline{u'v'}^2+\overline{w'v'}^2)^{1/2}$ and $q=2k=\overline{u_i'u_i'}$, decreases in 3DTBLs, and various structure models have been proposed to explain this inefficient extraction of shear stress from the same turbulence kinetic energy. This phenomenon can also be related to transition. It can be seen in Fig. 15 that a_1 decreases in a region close to the wall during pretransition, but starts increasing following the onset of transition, becoming significantly greater than that of the initial flow close to the wall on completion of the transition. Due to the higher new Reynolds number of the total flow, the profile of a_1 of the new flow is fuller closer to the wall. Away from the wall however, the a_1 deficit continues with a slightly increased strength and the region in which it occurs moves further into the core, which can be related to the fact that the new turbulence is still to propagate to this region, as discussed above.

The characteristic developments of turbulence stresses observed above for RE180P60 also appear in other 3DTBLs studied here with details varying in each case. The time developments of the maximum streamwise fluctuations for all cases studied here are compared in Fig. 16(a), which shows a trend of strengthening of the reduction in $\overline{u'^2}_{\max}$ with increasing transverse pressure gradient. Figure 16(b) shows that the combined effect of the applied transverse flow on all normal stresses is
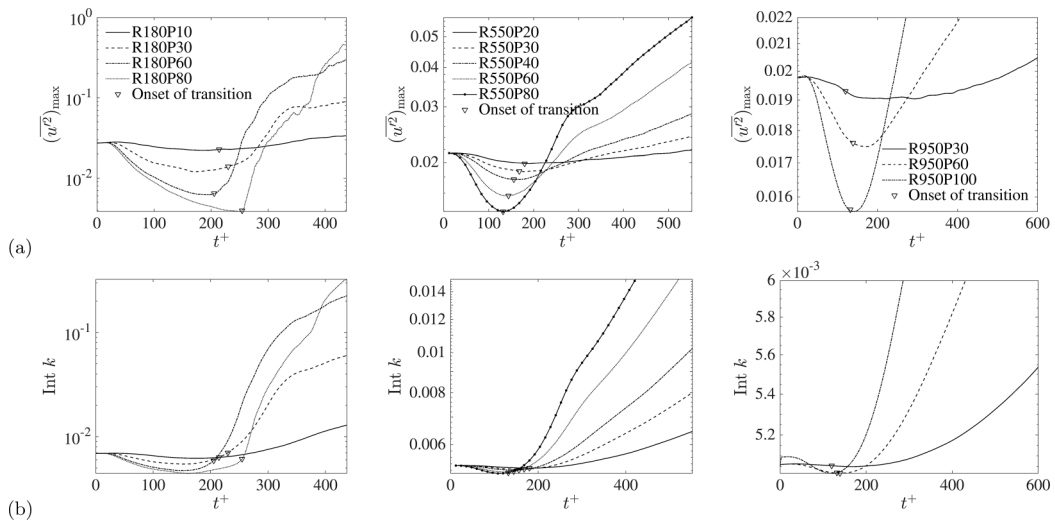
FIG. 16. Time development of (a) the maximum streamwise fluctuations and (b) the radial integral of the turbulence kinetic energy.

to cause the overall turbulence kinetic energy to decrease during pretransition despite the increase in $\overline{w'^2}$. This offers a different angle for the explanation of the reduction of turbulence as a key feature of the initial development of such nonequilibrium turbulence [14,15,27]. The reduction only occurs in the pretransition region [Fig. 16(a)]. It should be noted these values are normalized using the initial velocity, representing absolute changes with time. Since the spanwise flow rate increases significantly during this period, the turbulence intensity k/U_p^2 would be significantly lower than those shown in Fig. 16(a). The reduction in this relative quantity would occur in greater regions and over a longer time, well into the transition and the relaxation period showing the nonequilibrium nature of the flow.

We now analyze the energy growth of the turbulence (disturbances) from the point of view of transition. The rates of growth due to the transient growth and crossflow instability are characteristically different. The former normally undergoes an algebraic growth and the latter an exponential growth. The situation in flows where both mechanisms are present may be rather complex due to the combined effect of the two, as noted by Brandt *et al.* [50]. There is a further complication herein as the freestream velocity W_b increases continuously rather than being a constant as in most studies of transition.

Figure 14 shows that the most significant energy growth of disturbances is in the spanwise direction, aligning with the direction of the applied shear, while the streamwise and the wall-normal components actually decrease during this period for the reasons discussed earlier. Hence, we use the increase of the peak of the wall-normal profile of the spanwise fluctuating velocity to represent the energy growth,

$$\Delta \overline{w'^2} = \max_y [\overline{w'^2} - \overline{w'^2}(0)], \qquad (4)$$

which is shown in Fig. 17 in different normalizations. This quantity is normalized using W_b^2 as commonly done to show its relative increase with respect to the freestream velocity in Fig. 17(a). The square root velocity normalized as $(\Delta \overline{w'^2})^{1/2}/u_{\tau 0}a$ is plotted against t^+ in Fig. 17(b) and the displacement thickness Reynolds number based on friction velocity $\mathrm{Re}_{\tau \delta} = u_\tau \delta/\nu$ in Fig. 17(c). Here $a = W_b'(0)/(1/U_{b0})(\nu/u_{\tau 0}^2)$, where $W_b'(0) = (dW_b/dt)_{t=0}$, is an acceleration parameter used by He and Jackson [81] and this normalization illustrates the absolute development since both $u_{\tau 0}$ and a are constants during the transient process for each case.
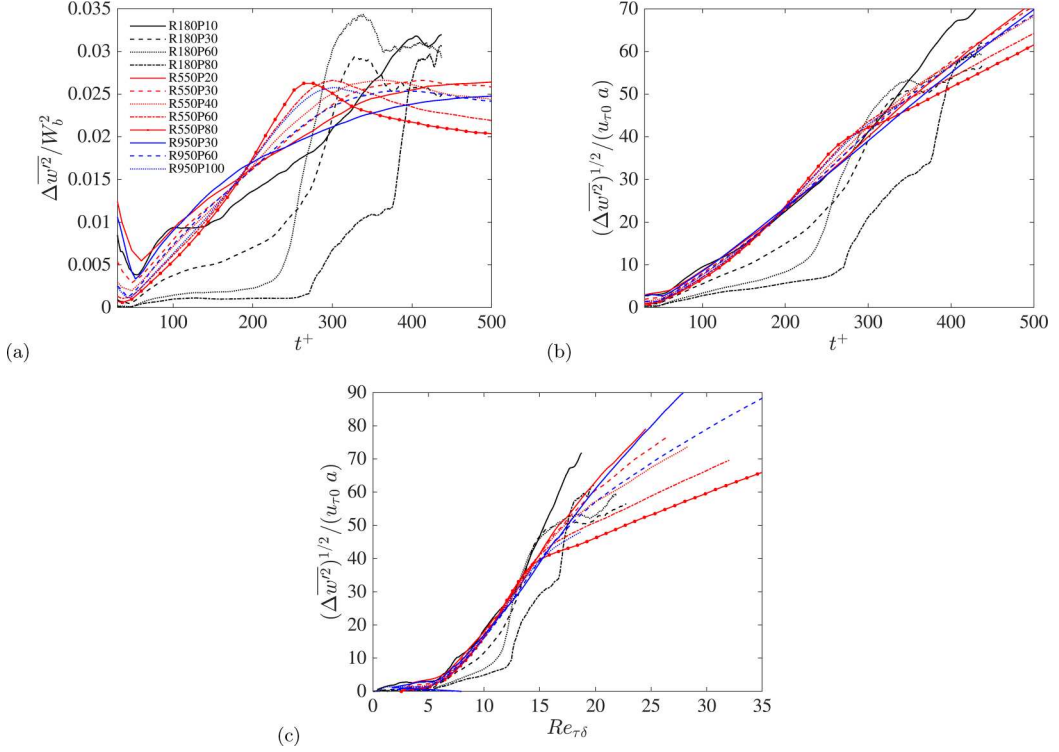
FIG. 17. Energy growth. (a) Spanwise energy growth $\Delta\overline{w'^2}$ normalized by the developing bulk velocity squared W_b^2. Also shown is the energy growth in the form of velocity normalized by the initial friction velocity and corrected by the acceleration parameter $(\Delta\overline{w'^2})^{1/2}/u_{\tau 0}a$, where $a = (dW_b/dt)_0(1/U_{b0})(\nu/u_{\tau 0}^2)$ [81], as a function of (b) time t^+ and (c) $\mathrm{Re}_{\tau\delta} = u_{\tau 0}\delta/\nu$.

It can be seen from Fig. 17 that group B cases show similar behaviors to each other, but group A cases show rather different behaviors from those of group B and also to some extent from each other. In group B, the growth of $\Delta\overline{w'^2}/W_b^2$ is largely linear during the pretransition period for cases with greater $\partial P/\partial z$, but becomes increasingly more curved with a faster initial growth and slower one later in the cases of lower $\partial P/\partial z$. In all cases of this group, on the completion of transition, $\Delta\overline{w'^2}/W_b^2$ would have reached a peak value at or above 0.24, which is typical of a turbulent flow, and it maintains this value or decreases slightly afterward. It can be seen from Fig. 17(b) that the absolute growths of $(\Delta\overline{w'^2})^{1/2}/u_{\tau 0}a$ in all group B cases are quite well correlated against t^+ and they are in even better agreement when plotted against the displacement thickness $\mathrm{Re}_{\tau\delta}$ in Fig. 17(c). Despite the excellent correlation between the different cases, the linear behavior $(\overline{w'^2})^{1/2}$ in this plot implies that the energy growth rate of $\overline{w'^2}$ is neither linear nor exponential. Finally, it is also interesting to note that the perturbation energy continues to increase after the completion of the transition, but this is likely due to the continuing increase of W_b.

The rate of disturbance energy growth $\Delta\overline{w'^2}/W_b^2$ in group A shown in Fig. 17(a) increases only at the early stages and then it remains largely unchanged until the onset of transition, after which a rapid increase occurs. The absolute growth in rms velocities shown in Figs. 17(b) and 17(c) is also significantly slower than those in group B. However, the development in Fig. 17(b) is close to $t^{1/2}$, that is, the energy $\Delta\overline{w'^2}$ shows a linear growth rate with time akin to that of transient (algebraic) growth in the bypass transition [42,49]. In those cases, since the disturbance energy at the onset
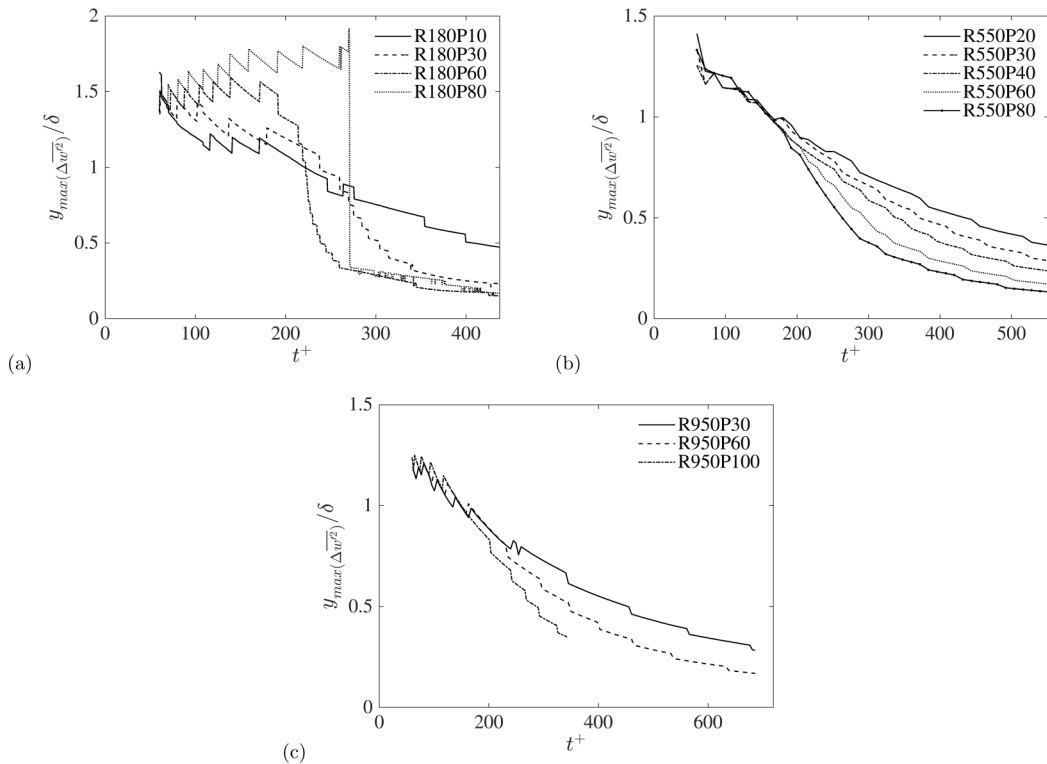
FIG. 18. Wall-normal location of the maximum growth of the spanwise fluctuating velocity $\Delta\overline{w'^2}$ relative to the displacement boundary thickness.

of transition is weak, it increases rapidly during the transition, reaching a value similar to those in group B on completion of the transition.

It is also interesting to note the different peak energy locations in groups A and B (Fig. 18). Normally the location normalized by the displacement thickness is expected to be around 1.3 in the pretransition region of the 2DBL transition and it decreases rapidly during the transition to a value around to 0.2 (or more precisely $y^+ = 15$) in the turbulent region [72]. The first value represents the location of the streaks and the latter the location of peak turbulence in a wall shear turbulent flow. It can be seen that the locations in group A cases largely follow this trend, though they appear to move outward somewhat in pretransition in R180P80 and the switch from the outer location to the near-wall one is a sudden drop. This is linked to the fact that $\overline{w'^2}$ has two peaks at this stage and the sudden change in location is due to the near-wall peak overtaking the outer-region peak, which occurs at some point during the transition. For cases in group B, the location appears to move more slowly towards the wall at a similar rate in each case until onset of transition, after which the cases with a larger $\partial P/\partial z$ decrease at a higher rate. This result may be interpreted as the pretransition energy growth in group B not being completely correlated with the spanwise boundary layer growth, but that it is influenced by crossflow instability.

IV. CONCLUSION

Insight into the nonequilibrium three-dimensional turbulent boundary layer has been established by analyzing data from direct numerical simulations. The three-dimensional flow results from an imposition of a transverse pressure gradient on an initial statistically stationary turbulent channel flow. A series of DNSs were analyzed including an initial flow at $Re_\tau = 186$, 546, and 934 and

a transverse pressure gradient up to 90 times that of the streamwise value. The transient response of the three-dimensional flow was shown to be characterized by the development of a laminarlike spanwise boundary layer followed by spontaneous transition to turbulence even though the initial flow is already turbulent. This phenomenon is similar to that found in a streamwise accelerating flow [23,24], comprising (i) a pretransition stage where the disturbances in the spanwise direction grow steadily (referred to as primary instability), (ii) a transition stage where turbulent spots are formed due to secondary instability and merge into each other and finally after the completion of the transition (i.e., the complete surface is covered by new turbulence), and (iii) a relaxation stage where the new turbulence, which is initially only in the near-wall region, gradually extends to the core of the flow. This last stage may take a relatively long time.

The cases studied here can be categorized into two groups: the low-Reynolds-number and high-transverse-flow cases ($Re_\tau = 180$ and the pressure ratio between 30 and 80, group A) and the rest of the cases (group B). For group B, the disturbance energy grows at a rate proportional to time squared and the onset of the transition to turbulence occurs when the relative crossflow velocity (the ratio between the primary velocity and the crossflow velocity) is strong, implying that crossflow instability is likely to play an important role in the transition. In group A cases, the crossflow initially develops rapidly but then remains largely unchanged during most of the pretransition, and hence the relative crossflow strength decreases due to the increase of the spanwise mean velocity during this period. For this group, the transition occurs at a time when the relative crossflow strength is weak, implying a dominant contribution from the transient growth mechanism. The overall energy growth is much weaker in group A than in group B.

In the early phase of the pretransition stage, the spanwise boundary layer follows closely the extended Stokes flow solution for laminar flow as indicated by the spanwise friction coefficient, the boundary layer thickness, and the shape factor. Towards the later stage of the pretransition, the friction coefficient and boundary layer thickness in the different cases can still be correlated with each other, but they deviate from the laminar profiles due to the effect of preexisting turbulence. This second pretransition stage is only observable in group B cases. The boundary layer grows much faster following the onset of the transition. As for a two-dimensional boundary layer transition, the equivalent transitional Reynolds number has been found to be inversely proportional to the freestream turbulence through a power-law relationship.

During the pretransition stage, the tilting of the streaks away from the streamwise direction and the sheltering effect due to the new spanwise boundary layer cause the streamwise and wall-normal stresses and the primary shear stress $-\overline{u'v'}$ to decrease significantly. This reduction overwhelms the energy growth in the spanwise direction and hence causes the overall turbulent kinetic energy as well as the structure parameter to decrease, explaining the observations made in previous studies of 3DTBLs. Such an effect is also responsible for the reduction of the friction coefficient in the streamwise direction.

[1] W. R. Schwarz and P. Bradshaw, Turbulence structural changes for a three-dimensional turbulent boundary layer in a 30 bend, J. Fluid Mech. **272**, 183 (1994).

[2] S. D. Anderson and J. K. Eaton, Reynolds stress development in pressure-driven three-dimensional turbulent boundary layers, J. Fluid Mech. **202**, 263 (1989).

[3] S. M. Ölçmen and R. L. Simpson, An experimental study of a three-dimensional pressure-driven turbulent boundary layer, J. Fluid Mech. **290**, 225 (1995).

[4] M. Furuya and H. Fujita, Turbulent boundary layer over rough gauze surfaces, Trans. Jpn. Soc. Mech. Eng. **32**, 724 (1966).

[5] L. R. Bissonnette and G. L. Mellor, Experiments on the behaviour of an axisymmetric turbulent boundary layer with a sudden circumferential strain, J. Fluid Mech. **63**, 369 (1974).

[6] R. P. Lohmann, The response of a developed turbulent boundary layer to local transverse surface motion, J. Fluid Eng. **98**, 354 (1976).

[7] D. M. Driver and S. K. Hebbar, Experimental study of a three-dimensional, shear-driven, turbulent boundary layer, AIAA J. **25**, 35 (1987).

[8] D. M. Driver and S. K. Hebbar, Three-dimensional shear-driven boundary-layer flow with streamwise adverse pressure gradient, AIAA J. **27**, 1689 (1989).

[9] S. Y. Jung and H. J. Sung, Characterization of the three-dimensional turbulent boundary layer in a concentric annulus with a rotating inner cylinder, Phys. Fluids **18**, 115102 (2006).

[10] H. S. Littell and J. K. Eaton, Turbulence characteristics of the boundary layer on a rotating disk, J. Fluid Mech. **266**, 175 (1994).

[11] X. Wu and K. D. Squires, Prediction and investigation of the turbulent flow over a rotating disk, J. Fluid Mech. **418**, 231 (2000).

[12] R. O. Kiesow and M. W. Plesniak, Modification of near-wall structure in a shear-driven 3-D turbulent boundary layer, J. Fluids Eng. **124**, 118 (2002).

[13] R. O. Kiesow and M. W. Plesniak, Near-wall physics of a shear-driven three-dimensional turbulent boundary layer with varying crossflow, J. Fluid Mech. **484**, 1 (2003).

[14] H. Abe, Direct numerical simulation of a non-equilibrium three-dimensional turbulent boundary layer over a flat plate, J. Fluid Mech. **902**, A20 (2020).

[15] P. Moin, T.-H. Shih, D. Driver, and N. Mansour, Direct numerical simulation of a three-dimensional turbulent boundary layer, Phys. Fluids **2**, 1846 (1990).

[16] O. Sendstad and P. Moin, On the mechanics of 3-D turbulent boundary layers, in *Proceedings of the Eighth Symposium on Turbulent Shear Flows, Munich* (U.S. DOE, Washington, DC, 1991).

[17] G. N. Coleman, J. Kim, and A.-T. Le, A numerical study of three-dimensional wall-bounded flows, Int. J. Heat Fluid Flow **17**, 333 (1996).

[18] A. Lozano-Durán, M. G. Giometto, G. I. Park, and P. Moin, Non-equilibrium three-dimensional boundary layers at moderate Reynolds numbers, J. Fluid Mech. **883**, A20 (2020).

[19] H. Fernholz and J.-D. Vagt, Turbulence measurements in an adverse-pressure-gradient three-dimensional turbulent boundary layer along a circular cylinder, J. Fluid Mech. **111**, 233 (1981).

[20] J. K. Eaton, Effects of mean flow three dimensionality on turbulent boundary-layer structure, AIAA J. **33**, 2020 (1995).

[21] J. Johnston and K. Flack, Advances in three-dimensional turbulent boundary layers with emphasis on the wall-layer regions, J. Fluids Eng. **118**, 219 (1996).

[22] G. Coleman, J. Kim, and P. Spalart, A numerical study of strained three-dimensional wall-bounded turbulence, J. Fluid Mech. **416**, 75 (2000).

[23] S. He and M. Seddighi, Turbulence in transient channel flow, J. Fluid Mech. **715**, 60 (2013).

[24] S. He and M. Seddighi, Transition of transient channel flow after a change in Reynolds number, J. Fluid Mech. **764**, 395 (2015).

[25] A. Mathur, S. Gorji, S. He, M. Seddighi, A. Vardy, T. O'Donoghue, and D. Pokrajac, Temporal acceleration of a turbulent channel flow, J. Fluid Mech. **835**, 471 (2018).

[26] B. Guerrero, M. F. Lambert, and R. C. Chin, Transient dynamics of accelerating turbulent pipe flow, J. Fluid Mech. **917**, A43 (2021).

[27] C. Kannepalli and U. Piomelli, Large-eddy simulation of a three-dimensional shear-driven turbulent boundary layer, J. Fluid Mech. **423**, 175 (2000).

[28] R. Antonia and R. Luxton, The response of a turbulent boundary layer to a step change in surface roughness part 1. smooth to rough, J. Fluid Mech. **48**, 721 (1971).

[29] K. Fukagata, K. Iwamoto, and N. Kasagi, Contribution of reynolds stress distribution to the skin friction in wall-bounded flows, Phys. Fluids **14**, L73 (2002).

[30] P. Bradshaw and N. Pontikos, Measurements in the turbulent boundary layer on an "infinite" swept wing, J. Fluid Mech. **159**, 105 (1985).

[31] R. J. Howard and N. D. Sandham, Simulation and modelling of a skewed turbulent channel flow, Flow, Turbul. Combust. **65**, 83 (2000).

[32] W.-J. Jung, N. Mangiavacchi, and R. Akhavan, Suppression of turbulence in wall-bounded flows by high-frequency spanwise oscillations, Phys. Fluids **4**, 1605 (1992).

[33] F. Laadhari, L. Skandaji, and R. Morel, Turbulence reduction in a boundary layer by a local spanwise oscillating surface, Phys. Fluids **6**, 3218 (1994).

[34] M. Quadrio and P. Ricco, Critical assessment of turbulent drag reduction through spanwise wall oscillations, J. Fluid Mech. **521**, 251 (1999).

[35] J. Eaton, Turbulence structure and heat transfer in three-dimensional boundary layers, in *Proceedings of the Ninth Symposium on Energy Engineering Sciences, Lemont* (U.S. DOE, Washington, DC, 1991).

[36] P. Klebanoff, Effect of free-stream turbulence on a laminar boundary layer, Bull. Am. Phys. Soc. **16**, 1323 (1971).

[37] L. N. Trefethen, A. E. Trefethen, S. C. Reddy, and T. A. Driscoll, Hydrodynamic stability without eigenvalues, Science **261**, 578 (1993).

[38] K. Westin, A. Boiko, B. Klingmann, V. Kozlov, and P. Alfredsson, Experiments in a boundary layer subjected to free stream turbulence. Part 1. Boundary layer structure and receptivity, J. Fluid Mech. **281**, 193 (1994).

[39] Y. S. Kachanov, Physical mechanisms of laminar-boundary-layer transition, Annu. Rev. Fluid Mech. **26**, 411 (1994).

[40] P. Durbin and X. Wu, Transition beneath vortical disturbances, Annu. Rev. Fluid Mech. **39**, 107 (2007).

[41] R. Jacobs and P. Durbin, Simulations of bypass transition, J. Fluid Mech. **428**, 185 (2001).

[42] P. Andersson, M. Berggren, and D. S. Henningson, Optimal disturbances and bypass transition in boundary layers, Phys. Fluids **11**, 134 (1999).

[43] L. Brandt and D. S. Henningson, Transition of streamwise streaks in zero-pressure-gradient boundary layers, J. Fluid Mech. **472**, 229 (2002).

[44] T. A. Zaki and P. A. Durbin, Mode interaction and the bypass route to transition, J. Fluid Mech. **531**, 85 (1999).

[45] J. Hœpffner and L. Brandt, Stochastic approach to the receptivity problem applied to bypass transition in boundary layers, Phys. Fluids **20**, 024108 (2008).

[46] P. Schlatter, L. Brandt, H. De Lange, and D. S. Henningson, On streak breakdown in bypass transition, Phys. Fluids **20**, 101505 (2008).

[47] P. Ricco, J. Luo, and X. Wu, Evolution and instability of unsteady nonlinear streaks generated by free-stream vortical disturbances, J. Fluid Mech. **677**, 1 (2011).

[48] N. J. Vaughan and T. A. Zaki, Stability of zero-pressure-gradient boundary layer distorted by unsteady Klebanoff streaks, J. Fluid Mech. **681**, 116 (2011).

[49] P. Luchini, Reynolds-number-independent instability of the boundary layer over a flat surface: Optimal perturbations, J. Fluid Mech. **404**, 289 (2000).

[50] L. Brandt, P. Schlatter, and D. S. Henningson, Transition in boundary layers subject to free-stream turbulence, J. Fluid Mech. **517**, 167 (1999).

[51] J. H. Fransson, L. Brandt, A. Talamelli, and C. Cossu, Experimental study of the stabilization of Tollmien-Schlichting waves by finite amplitude streaks, Phys. Fluids **17**, 054110 (2005).

[52] S. Nagarajan, S. Lele, and J. Ferziger, Leading-edge effects in bypass transition, J. Fluid Mech. **572**, 471 (2007).

[53] V. Ovchinnikov, M. M. Choudhari, and U. Piomelli, Numerical simulations of boundary-layer bypass transition due to high-amplitude free-stream turbulence, J. Fluid Mech. **613**, 135 (2008).

[54] H. L. Reed and W. S. Saric, Stability of three-dimensional boundary layers, Annu. Rev. Fluid Mech. **21**, 235 (1989).

[55] H. L. Reed, W. S. Saric, and D. Arnal, Linear stability theory applied to boundary layers, Annu. Rev. Fluid Mech. **28**, 389 (1996).

[56] H. Bippes, Basic experiments on transition in three-dimensional boundary layers dominated by crossflow instability, Prog. Aerosp. Sci. **35**, 363 (1999).

[57] W. S. Saric, H. L. Reed, and E. B. White, Stability and transition of three-dimensional boundary layers, Annu. Rev. Fluid Mech. **35**, 413 (2003).

[58] M. R. Malik, F. Li, M. M. Choudhari, and C.-L. Chang, Secondary instability of crossflow vortices and swept-wing boundary-layer transition, J. Fluid Mech. **399**, 85 (1999).

[59] E. B. White and W. S. Saric, Secondary instability of crossflow vortices, J. Fluid Mech. **525**, 275 (1999).

[60] G. Bonfigli and M. Kloker, Secondary instability of crossflow vortices: Validation of the stability theory by direct numerical simulation, J. Fluid Mech. **583**, 229 (2007).

[61] P. Corbett and A. Bottaro, Optimal linear growth in swept boundary layers, J. Fluid Mech. **435**, 1 (2001).

[62] L.-U. Schrader, S. Amin, and L. Brandt, Transition to turbulence in the boundary layer over a smooth and rough swept plate exposed to free-stream turbulence, J. Fluid Mech. **646**, 297 (2010).

[63] M. P. Hack and T. A. Zaki, Modal and non-modal stability of boundary layers forced by spanwise wall oscillations, J. Fluid Mech. **778**, 389 (2015).

[64] M. Seddighi, S. He, D. Pokrajac, T. O'Donoghue, and A. Vardy, Turbulence in a transient channel flow with a wall of pyramid roughness, J. Fluid Mech. **781**, 226 (2015).

[65] A. Mathur, M. Seddighi, and S. He, Transition of transient channel flow with high Reynolds number ratios, Entropy **20**, 375 (2018).

[66] L. J. Sundstrom and M. J. Cervantes, On the similarity of pulsating and accelerating turbulent pipe flows, Flow, Turbul. Combust. **100**, 417 (2018).

[67] L. J. Sundstrom and M. J. Cervantes, Laminar similarities between accelerating and decelerating turbulent flows, Int. J. Heat Fluid Flow **71**, 13 (2018).

[68] S. Y. Jung and K. Kim, Transient behaviors of wall turbulence in temporally accelerating channel flows, Int. J. Heat Fluid Flow **67**, 13 (2017).

[69] A. Lozano-Durán, M. J. P. Hack, and P. Moin, Modeling boundary-layer transition in direct and large-eddy simulations using parabolized stability equations, Phys. Rev. Fluids **3**, 023901 (2018).

[70] H. J. Bae, A. Lozano-Duran, S. T. Bose, and P. Moin, Turbulence intensities in large-eddy simulation of wall-bounded flows, Phys. Rev. Fluids **3**, 014610 (2018).

[71] G. N. Coleman, J. Kim, and P. R. Spalart, Direct numerical simulation of strained three-dimensional wall-bounded flows, Exp. Therm. Fluid Sci. **13**, 239 (1996).

[72] M. Matsubara and P. H. Alfredsson, Disturbance growth in boundary layers subjected to free-stream turbulence, J. Fluid Mech. **430**, 149 (2001).

[73] X. Wu, P. Moin, J. M. Wallace, J. Skarda, A. Lozano-Durán, and J.-P. Hickey, Transitional-turbulent spots and turbulent-turbulent spots in boundary layers, Proc. Natl. Acad. Sci. **114**, E5292 (2017).

[74] H. Schlichting and K. Gersten, *Boundary-Layer Theory* (Springer, Berlin, 2016).

[75] S. He and C. Ariyaratne, Wall shear stress in the early stage of unsteady turbulent pipe flow, J. Hydraul. Eng. **137**, 606 (2011).

[76] S. He, C. Ariyaratne, and A. Vardy, Wall shear stress in accelerating turbulent pipe flow, J. Fluid Mech. **685**, 440 (2011).

[77] J. H. Fransson, M. Matsubara, and P. H. Alfredsson, Transition induced by free-stream turbulence, J. Fluid Mech. **527**, 1 (1999).

[78] H. B. Kurz and M. J. Kloker, Mechanisms of flow tripping by discrete roughness elements in a swept-wing boundary layer, J. Fluid Mech. **796**, 158 (2016).

[79] J. Hunt and P. Durbin, Perturbed vortical layers and shear sheltering, Fluid Dyn. Res. **24**, 375 (1999).

[80] T. A. Zaki and S. Saha, On shear sheltering and the structure of vortical modes in single-and two-fluid boundary layers, J. Fluid Mech. **626**, 111 (2009).

[81] S. He and J. Jackson, A study of turbulence under conditions of transient flow in a pipe, J. Fluid Mech. **408**, 1 (2000).